Research Square

Preprints are preliminary reports that have not undergone peer review.
They should not be considered conclusive, used to inform clinical practice,
or referenced by the media as validated information.

China's oldest rocks reveal 3.95 Ga subduction and Hadean mantle depletion

Hangqiang Xie

rockshrimp@126.com

Institute of Geology, Chinese Academy of Geological Schences

Chunyan Dong

Institute of Geology, Chinese Academy of Geological Schences

Pengchuan Li

College of Earth Sciences, Jilin University

Rongfeng Ge

Nanjing University https://orcid.org/0000-0001-5690-9289

Simon Wilde

Curtin University https://orcid.org/0000-0002-4546-8278

Shoujie Liu

Institute of Geology, Chinese Academy of Geological Schences

Dunyi Liu

The Beijing SHRIMP Center, Institute of Geology, Chinese Academy of Geological Sciences, Beijing 100037, China.

Yusheng Wan

Institute of Geology, Chinese Academy of Geological Schences

Physical Sciences - Article

Keywords:

Posted Date: June 8th, 2026

DOI: https://doi.org/10.21203/rs.3.rs-9401592/v1

License: This work is licensed under a Creative Commons Attribution 4.0 International License.
Read Full License

Additional Declarations: There is **NO** Competing Interest.

Version of Record: A version of this preprint was published at Nature on November 11th, 2026. See the published version at https://doi.org/10.1038/s41586-026-11280-2.

China's oldest rocks reveal 3.95 Ga subduction and Hadean mantle depletion

Hangqiang Xie[1*], Chunyan Dong[1], Pengchuan Li[2], Rongfeng Ge[3], Simon A. Wilde[4], Shoujie Liu[1], Dunyi Liu[1], Yusheng Wan[1*]

1 Beijing SHRIMP Center, Institute of Geology, Chinese Academy of Geological Sciences, Beijing 100037, China
2 College of Earth Sciences, Jilin University, Changchun 130061, China
3 State Key Laboratory of Critical Earth Material Cycling and Mineral Deposits, Institute of Continental Geodynamics, Frontiers Science Center for Critical Earth Material Cycling, School of Earth Sciences and Engineering, Nanjing University, Nanjing 210023, PR China
4 School of Earth and Planetary Sciences, Curtin University, GPO Box U1987, Perth 6854, WA, Australia

The scarcity of terrestrial rocks older than 3.9 billion years (Ga) has hindered our understanding of Earth's early evolution, fueling persistent debates on how and when the first continental crust formed and plate tectonics started. Currently, the only unequivocally documented >3.9 Ga rocks are from the Acasta Gneiss Complex, Canada [1–3]. Here we report a newly discovered 3.95 Ga trondhjemitic gneiss from eastern Hebei, North China Craton, where 3.95 Ga magmatic zircon records elevated $\delta^{18}O$ values (average +6.77 ± 0.23‰) and positive $\varepsilon_{Hf}(t)$ (weighted mean +1.45 ± 0.27), indicating a low-temperature altered basaltic source that originated from a Hadean depleted mantle. In contrast to the low-pressure origin inferred for the ca. 4.0 Ga Acasta rocks [2], the 3.95 Ga trondhjemitic gneiss reported here exhibits geochemical signatures attributed to a high-pressure origin [4]. Thermodynamic and trace element modelling demonstrates that its parental magma formed via low degree (8–16%) melting of basaltic crust at >1.6 GPa and 740–820 °C, suggesting rapid burial of (near-)surface-altered oceanic crust to mantle depths along a cool thermal gradient. We propose that this rapid burial was most likely achieved through a transient subduction event.

Understanding Earth's earliest crustal evolution requires direct evidence from its oldest surviving rocks. Although Hadean detrital zircon provides mineral-scale insights, Eoarchean rocks provide systematic petrological, geochemical, geochronological, and isotopic records essential for reconstructing crust-forming processes. However, there is usually controversy about the Sm/Nd isochron dating of mafic-ultramafic rocks, with the well-known example being the Nuvvuagittuq Greenstone Belt that has been proposed to represent Hadean crust [5,6], although associated rocks record U-Pb zircon ages of 3.77 Ga [7]. On the contrary, zircon U-Pb dating of early Archean granitoids, commonly metamorphosed to felsic gneisses, generally yields reliable crystallization ages. The oldest unequivocally dated rock remains the 4031 ± 3 Ma Acasta gneiss

(Slave Craton, Northwest Territories of Canada [1,2]). Slightly younger Eoarchean (3.9–3.7 Ga) gneisses are documented in Labrador (Canada) [8,9], West Greenland [10], East Antarctica [11], and China [12,13], yet no rocks older than 3.9 Ga have been confirmed other than the Acasta gneiss.

The rarity of >3.9 Ga rocks on Earth has resulted in considerable uncertainties on the formation mechanism and geodynamic setting of the earliest crust. The best-preserved samples of the 4.03–4.02 Ga Acasta gneiss exhibit flat rare earth element (REE) patterns and negative Eu anomalies, indicating a shallow crustal origin, potentially by low-pressure magma fractionation in an Iceland-like setting dominated by mantle upwelling [3], or partial melting induced by impacts [14]. In contrast, most 3.9–3.7 Ga gneisses worldwide are rocks of the tonalite–trondhjemite–granodiorite (TTG) suite, with geochemical features (e.g., high Na_2O/K_2O ratios and low heavy REE (HREE), Y, Nb, Ta and Ti contents) indicating partial melting of hydrated mafic sources at pressures sufficiently high to stabilize garnet and suppress plagioclase (≥0.8–1.0 GPa [4]). Recent thermodynamic–geochemical modelling indicates that some Eoarchean TTGs were formed at high-pressures by rapid burial of basaltic crust to mantle depths, suggesting operation of subduction–accretion tectonics by at least 3.7 Ga [13]. Nevertheless, whole-rock geochemical proxies for melting pressures may be complicated by magmatic processes, such as crystal fractionation and accumulation [15,16]. Critically, whether high-pressure TTGs older than 3.9 Ga ever existed remains an open question, leaving the nature of pre-3.9 Ga crustal dynamics unresolved.

A related issue concerns the timing and extent of early crust-mantle differentiation. Extraction of crust via mantle melting would produce a complementary depleted mantle (DM) reservoir. This process would fractionate Sm/Nd and Lu/Hf, leaving the mantle with higher ratios than the crust. Subsequent radioactive decay of Sm and Lu would thus yield distinct isotopic signatures: positive $\varepsilon_{Nd}(t)$ and $\varepsilon_{Hf}(t)$ in rocks derived from a DM and negative values in rocks derived from older crust. While recent studies have documented negative $\varepsilon_{Nd}(t)$ and $\varepsilon_{Hf}(t)$ values in early Archean rocks, suggesting Hadean crustal antecedents [5,17–20], evidence for Hadean DM remains debated. Widespread positive ^{142}Nd anomalies observed in many Archean rocks [21–24] have been interpreted as evidence for Hadean mantle depletion, because ^{142}Nd is the decay product of short-lived ^{146}Sm (half-life ~103 Ma) [25], which would have effectively been extinct by 4.0 Ga if mantle depletion occurred later. However, positive $\varepsilon_{Hf}(t)$ values are scarce in Hadean-Eoarchean zircons, casting doubts on whether Hadean mantle was substantially depleted [26]. Reconciling these conflicting Nd and Hf isotopic records is critical for understanding early differentiation of the Earth.

Here, we report a 3.95 Ga trondhjemitic gneiss in the Shimen Complex newly discovered in eastern Hebei, North China Craton [18]. As second oldest only to the Acasta rocks, it provides a rare opportunity to probe early crustal processes. Importantly, its geochemical and isotopic compositions indicate an origin involving high pressure partial melting of basaltic crust derived from Hadean DM. This discovery provides critical new insights into the mechanisms of crustal formation and dynamics in the early Earth.

Geological Setting and Sample Descriptions

The Shimen Complex is located in the Labashan area of eastern Hebei, and occurs within undeformed 2.5 Ga potassic granite as enclaves ranging from a few meters to over a hundred meters long (Figs. S1a-c). The complex comprises both supracrustal rocks and igneous rocks [18]. The supracrustal rocks are mainly composed of meta-basalt-ultramafic rocks and meta-sedimentary rocks with ages between 3.5 Ga (the youngest detrital zircon) and 3.1 Ga (metamorphic zircon), whereas the igneous rocks are mainly composed of 3.84–3.1 Ga TTG/granitic gneisses and meta-gabbro, together with the newly identified 3.95 Ga trondhjemitic gneiss reported here. The supracrustal rocks and granitoids are in tectonic contact owing to strong deformation.

The 3.95 Ga trondhjemitic gneiss occurs in the largest enclave (N39°46′40″, E118°51′29″; Fig. S1c) on a steep slope and crops out ca. 15 m^2. It is juxtaposed against a 3.5 Ga granitic gneiss and is intruded by a 2.5 Ga syenogranite (Fig. S2a). Three samples were collected for detailed analysis. Sample J2212 was obtained from banded trondhjemitic gneiss in the central portion (Figs. S2a, b), and contains millimeter-scale light-colored layers interpreted as deformed thin granitic veins that could not be completely separated during the sampling process. Samples J2302 and J2303 were taken from relatively homogenous trondhjemitic gneiss in the upper and lower part of the outcrop, respectively, where a few younger veins were removed prior to analysis (Figs. S2a, c, d). The trondhjemitic gneisses (J2302, J2303) have a granoblastic texture and are similar in mineral association, consisting mainly of quartz (30–35%), plagioclase (55–65%), K-feldspar (3–6%) and biotite (3–10%) (Figs. S3a, b), although biotite content is lower in sample J2303. In banded trondhjemite gneiss sample J2212, layers with higher microcline content (Fig. S3c, bottom right) are interpreted as deformed monzogranitic veins.

Zircon U-Pb Geochronology, O-Hf Isotopes and Trace Elements

Zircon U-Pb dating was performed on all three samples using a sensitive high resolution ion microprobe (SHRIMP) (Methods, Table S1). The zircon grains from all samples have similar morphology, internal structure and U-Pb age pattern, consistent with a cogenetic origin. Cathodoluminescence (CL) images reveal many zircons have core-rim structures (Figs. 1a-c, S4). The cores usually have well-preserved oscillatory zoning or parallel banding, indicating a magmatic origin (named here as 'magmatic zircon'). However, zoning is blurred or obliterated in a few cores and many of the rims, typical characteristic of recrystallization (named here as 'recrystallized zircon'). There are also some newly-formed zircons, particularly in sample J2302, which occur as overgrowth rims or small individual grains and are characterized by anhedral form and the absence of internal structure, suggesting a metamorphic origin (Fig. 1a, S4). The concordant analyses on 11 magmatic/recrystallized cores and 9 newly-formed zircons from sample J2302 yielded weighted mean $^{207}Pb/^{206}Pb$ ages of 3948 ± 5 Ma (95% confidence level, MSWD = 1.3, n = 11) and 3450 ± 7 Ma (MSWD = 1.4, n = 9) (Figs. 1d, S5a), interpreted respectively as the magma crystallization and metamorphic ages. Similarly, the oldest concordant analyses on magmatic/recrystallized cores from samples J2303 and J2212 yielded weighted mean $^{207}Pb/^{206}Pb$ ages of 3951 ± 6 Ma

(MSWD = 1.5, n = 10) and 3954 ± 5 Ma (MSWD = 0.69, n = 12), indicating all samples formed coevally at 3.95 Ga (Figs. 1e, f, S5b, c). Collectively, the weighted mean age of 3951 ± 3 Ma (MSWD = 1.15) given by 33 concordant analyses from all three samples is considered the best estimate of the crystallization age (Fig. S5d). Importantly, the homogenous samples J2302 and J2303 contain few <3.9 Ga concordant magmatic zircons, suggesting a simple crystallization history. In contrast, the banded gneiss (sample J2212) contains a few magmatic zircons with concordant ages of 3.86–3.70 Ga, which are attributed to either crystallization from the thin granitic veins or ancient radiogenic Pb (Pb*) loss from 3.95 Ga zircons. Concordant ages of 3.91–3.43 Ga are also recorded in some recrystallized zircons in J2302 and J2303, which are explained as partial or complete resetting of the U-Pb system of the 3.95 Ga zircons during the 3.45 Ga metamorphic event. The other analyses are discordant, likely due to variable degrees of Pb* loss at different periods (Fig. S5).

After repolishing, *in-situ* zircon O isotope analysis was performed at the same locations as the U-Pb analyses (Methods, Table S2). The ca. 3.95 Ga primary magmatic zircon cores have $\delta^{18}O$ values from 5.62 to 7.97‰, with an average of 6.77 ± 0.23‰ (2SE, n = 24, Fig. 2a), higher than the mantle zircon $\delta^{18}O$ value (5.3 ± 0.6‰, 2SD [27]), indicating either low-temperature hydrothermal alteration of the source rock or incorporation of supracrustal materials into the parental magmas. Thus, the source rocks of the 3.95 Ga trondhjemitic gneiss must have undergone surface or near-surface processes prior to partial melting. The other zircons (younger magmatic, recrystallized, newly-formed zircons and discordant magmatic zircons) commonly have similar $\delta^{18}O$ values, but a few grains/domains have lower $\delta^{18}O$ (down to 4.0 ‰), suggesting possible interaction with low $\delta^{18}O$ fluids during later alteration.

The primary magmatic/recrystallized zircons with >3.9 Ga $^{207}Pb/^{206}Pb$ ages have homogeneous initial Hf isotopic compositions, with ε_{Hf} (t = 3.95 Ga) values ranging from +0.28 to +2.83 with a weighted mean of 1.41 ± 0.44 (95% confidence level, n = 18, MSWD = 1.3) in the first analytical session, and from +0.66 to +2.42 with a weighted mean of 1.47 ± 0.45 (n = 8, MSWD = 2.1) in the second session (see Methods and Table S3). The weighted mean of +1.45 ± 0.27 (MSWD = 1.5) for all 26 analyses is considered the best estimate of the initial magmatic Hf isotope composition. The uniformly positive ε_{Hf} (t) values indicate that the 3.95 Ga trondhjemitic gneiss was derived from a juvenile source that was extracted from a DM that was in existence in the Hadean (Fig. 2b). It is worth noting that the magmatic and recrystallized zircons with <3.9 Ga $^{207}Pb/^{206}Pb$ ages in J2302 and J2303 also have the similar $^{176}Hf/^{177}Hf$ ratios (Fig. S6), which is consistent with the explanation that these younger ages are the result of Pb* loss or U-Pb system resetting of 3.95 Ga zircons, since the Hf isotope composition is usually unaffected during Pb* loss and recrystallization [28]. Newly-formed zircons and younger magmatic/recrystallized zircons in J2212 yield similar or slightly higher $^{176}Hf/^{177}Hf$ ratios (Fig. S6), suggesting incorporation of variable amounts of radiogenic Hf during the formation of these zircon domains.

In-situ zircon trace element analyses (Methods) yield a range of compositions (Table S4 and Figs. S7a-c). After filtering, the 3.95 Ga magmatic zircons are characterized by low Ti contents (average 6.2 ppm), positive Ce anomalies and negative

Eu anomalies. Using the zircon oxybarometer–hygrometer [32] (Table S5), the magmatic oxygen fugacity (fO_2) and H_2O contents of the 3.95 trondhjemitic gneiss are estimated to range from -1.39 to 0.27 (relative to the fayalite–magnetite–quartz buffer, or ΔFMQ; average -0.65) and 8.5 to 9.1 wt%, respectively. Ge et al. [32] suggested that the magmatic fO_2, H_2O content increased during the Eoarchean, and the appearance of wet and oxidizing magmas marked the onset of subduction. Our values fall at the upper end of ranges reported for Eoarchean (4.0–3.6 Ga) granitoids and may record the early stage of this increase [32] (Table S5 and Figs. S7d, e).

Whole-rock Geochemistry

The trondhjemitic gneiss samples (J2302, J2303) exhibit typical Archean TTG compositions (Table S6, Fig. 3), plotting in the trondhjemite field in the anorthite (An)–albite (Ab)–orthoclase (Or) diagram (Fig. S8a). The banded gneiss (sample J2212) has a higher K_2O content, plotting in the granite field, likely due to the influence of the thin granitic veins. All samples share distinctive high-pressure TTG trace element signatures: high Sr and low Y, HREE, Nb, Ta, and Ti concentrations, without negative Eu anomalies. These geochemical features are markedly different from those of the 4.03–4.02 Ga Acasta gneiss (Fig. 3) and most ca. 3.8 Ga TTGs, but do show affinities with the 3.72 Ga Aktash gneiss in the Tarim Craton (Figs. S8b-d), suggesting a similar high-pressure origin.

Thermodynamic and Trace Element Modelling

To constrain the formation conditions of the parental magma of the 3.95 Ga trondhjemitic gneiss, we carried out thermodynamic modelling to examine partial melting of the basaltic protolith. Based on a compilation of the oldest meta-mafic rocks worldwide (see Methods and Table S7), amphibolite group I from the Acasta Complex [33] was selected as the composition of the most plausible source rock (Figs. S9a, b). Modelling confirms that the Sr, Nb-Ta, and HREE concentrations in the melt are sensitive to melting pressure, whereas the abundance of large-ion lithophile elements (LILE; e.g., K, Cs, Rb, Ba, Th, U) and light REEs (LREE) is mainly controlled by the degree of partial melting. Low-degree partial melting at high-pressure conditions is required to reproduce the geochemical features of the 3.95 Ga trondhjemitic gneiss, including pronounced LREE/HREE fractionation, and strong negative Nb-Ta anomalies and positive Sr anomalies. The average composition of the homogeneous samples J2302 and J2303 is well matched with melts generated by 8–16% partial melting at >1.6 GPa and 740–860 °C, with the best fit at ~1.7 GPa and ~800 °C (Fig. 4a). These conditions correspond to a melting depth of >50 km and a low thermal gradient of <540 °C/GPa (equivalent to <17 °C/km). This thermal gradient is much lower than that inferred for most Eoarchean TTGs, but aligns with estimates for the 3.72 Ga tonalitic gneiss in the Tarim Craton (Fig. 4b). The diversity in estimated formation pressures of Eoarchean TTGs worldwide highlights substantial heterogeneity in formation processes and dynamic settings. Although high-pressure geochemical signatures of TTG can also be generated at moderate pressures via amphibole fractionation or plagioclase accumulation [16,34], such a model is inconsistent with our

observations from the 3.95 Ga trondhjemitic gneiss. Firstly, amphibole fractionation requires a dioritic (sanukitoid-like) parental magma, which is absent in the early Archean geological record. Secondly, extensive amphibole fractionation would deplete middle REEs (MREE) relative to HREE, resulting in low Gd_N/Yb_N ratios [35], contrary to the high Gd_N/Yb_N ratios (5–6) of the 3.95 Ga trondhjemitic gneiss in the Shimen Complex. Thirdly, plagioclase accumulation would result in positive Eu anomalies coupled with lower whole-rock SiO_2, which is not observed. Thus, a high-pressure melting origin is the most plausible explanation for the 3.95 Ga trondhjemitic gneiss.

Implications for Hadean crust and mantle differentiation

The 3.95 Ga trondhjemitic gneiss has a distinct positive $\varepsilon_{Hf}(t)$ signature, with a weighted mean of +1.45 ± 0.27. This requires a juvenile basaltic precursor derived from a DM that likely formed prior to 4.3 Ga (later mantle depletion requires unrealistically high $^{176}Lu/^{177}Hf$ to explain the observed $\varepsilon_{Hf}(t)$ values, Fig. S10), implying extensive crustal growth in the Hadean. In contrast, magmatic zircons from 3.8–3.6 Ga TTG gneisses within the same complex have negative $\varepsilon_{Hf}(t)$ values (averages ranging from -1.46 ± 0.65 to -3.49 ± 0.92) (Dong et al., 2024), which are too negative to share the juvenile source with the 3.95 Ga rocks, and too close to chondrite to be derived from the mafic crust extracted from the mantle before 4.3 Ga. The large $\varepsilon_{Hf}(t)$ variations of the 3.95–3.6 Ga zircons suggest that the basaltic precursors were derived from variable mantle sources and at different times. This Hf isotopic diversity in eastern Hebei can be reconciled through a multi-stage crust-mantle evolution model: (1) Early basaltic crust extraction from the mantle before 4.3 Ga generated a DM; (2) subsequent recycling of Hadean crust into the mantle partially re-homogenized Hadean DM, creating mantle heterogeneity; (3) at ~3.95 Ga, renewed melting of isolated >4.3 Ga DM generated mafic rocks, which were rapidly re-melted to produce the 3.95 Ga trondhjemitic gneiss; and (4) the 3.8–3.6 Ga TTG magmas were derived from basaltic rocks of diverse ages and compositions.

Similar to the 3.8–3.6 Ga TTG magmas in eastern Hebei, negative zircon $\varepsilon_{Hf}(t)$ values are widespread in Eoarchean-Paleoarchean rocks [17,19] and Hadean detrital zircons [36]. Together with negative ^{142}Nd anomalies in many Archean terrains [5,20], these negative $\varepsilon_{Hf}(t)$ values affirm the existence of extensive Hadean crust, the complementary reservoir to Hadean DM. However, precise evidence for Hadean DM in the form of positive zircon $\varepsilon_{Hf}(t)$ values has remained scarce, leading some workers to propose that major mantle depletion commenced only after ca. 3.8 Ga [26].

Positive whole-rock ^{142}Nd anomalies have also been identified in many Eoarchean to Paleoarchean rocks [21–24], whereas positive zircon $\varepsilon_{Hf}(t)$ values, although scarce, have been reported in a few samples from Isua (W. Greenland [37,38]) and Anshan [39], This supports the existence of a Hadean DM, which is also substantiated by the highly unradiogenic Sr isotopic compositions of olivine-hosted melt inclusions in 3.27 Ga komatiite [40]. Apparent decoupling between zircon Hf and whole-rock ^{142}Nd isotopes in some Archean rocks likely stems from the fact that all zircon-bearing rocks identified so far are formed after the extinction of ^{146}Sm at the end of the Hadean, whereas ^{142}Nd anomalies can be inherited from earlier differentiation events. The rarity of positive

$\varepsilon_{Hf}(t)$ records in Hadean-Eoarchean zircons is also likely related to efficient crustal recycling and mantle mixing in the hot early Earth [41], which would dilute or erase Hf isotopic signals of a DM. Preservation of a positive zircon $\varepsilon_{Hf}(t)$ signal requires a specific scenario: (1) the DM formed in the Hadean were isolated from later crustal recycling; (2) basaltic precursors were derived from the surviving Hadean DM; and (3) partial melting occurred shortly after the formation of the basaltic precursors to form TTG containing zircons. Therefore, it is natural that positive zircon $\varepsilon_{Hf}(t)$ values recording Hadean DM are rarely preserved since all the above three points need to be met. Our new data, with a distinct positive $\varepsilon_{Hf}(t = 3.95\ Ga)$ signature with a weighted mean of $+1.45 \pm 0.27$, provide a rare, definitive evidence for the presence of a Hadean DM.

Geodynamic Implications

The petrogenesis and tectonic setting of the 3.95 Ga trondhjemitic gneiss in the Shimen Complex are constrained by three key lines of evidence: (1) Positive zircon $\varepsilon_{Hf}(t)$ values indicate rapid melting of juvenile basaltic crust derived from a $\geq$4.3 Ga DM reservoir; (2) Elevated zircon $\delta^{18}O$ values indicate that the basaltic precursor suffered low-temperature hydrothermal alteration; (3) Thermodynamic–geochemical modelling indicates that partial melting occurred at high pressure (~1.7 GPa) under a low geothermal gradient. Collectively, these constraints demand a mechanism that can rapidly transport (near-)surface-altered oceanic crust to depths exceeding 50 km. This provides the first petrological evidence for such deep burial of near-surface materials as early as 3.95 Ga. Subduction offers the most coherent explanation for our combined dataset, while other explanations face greater challenges. For example, partial melting of thickened or delaminated lower crust of an oceanic plateau fails to account for the required surface or near-surface alteration of the source and low geothermal gradient considering the hot mantle in the early Archean [42,43]. Gravity-driven "dripping" (i.e., sagduction) of mafic–ultramafic volcanic rocks [44] requires pre-existing felsic crust on a relatively large scale to provide a density contrast, so cannot be used to explain the oldest rocks documented here. The Heat pipe model [45] involves frequent global volcanic resurfacing and efficient crustal recycling and mantle mixing, therefore struggles to explain preservation of ancient crust and Hadean DM. Instead, recent geodynamic modelling [40] suggests that frequent, short-lived subduction, possibly triggered by large-scale mantle upwelling [46,47] or impact [48], was likely responsible for crustal growth and mantle differentiation in the early Earth. A subduction origin of the 3.95 Ga trondhjemitic gneiss is supported by the relatively high magmatic fO_2 and H_2O relative to the slightly older Acasta gneiss, and an increasing trend is proposed to be linked to the onset of subduction [32]. Therefore, we propose that the 3.95 Ga trondhjemitic gneiss provides the first evidence for such transient subduction in early Earth's rock record.

The 3.95 Ga trondhjemitic gneiss not only ranks among Earth's oldest known rocks but also preserves a unique isotopic and geochemical fingerprint of Hadean mantle depletion and Eoarchean deep crustal processes. Its formation necessitates rapid burial and melting of (near-)surface-altered oceanic crust, likely through an early, transient subduction mechanism. This discovery provides a critical petrological and

geochemical benchmark for testing models of early Earth geodynamics and crust-mantle evolution.

References

1 Bowring, S. A. & Williams, I. S. Priscoan (4.00–4.03Ga) orthogneisses from northwestern Canada. *Contrib. Mineral. Petrol.* **134**, 3–16 (1999).

2 Reimink, J. R., Chacko, T., Stern, R. A. & Heaman, L. M. The birth of a cratonic nucleus: Lithogeochemical evolution of the 4.02–2.94Ga Acasta Gneiss Complex. *Precambrian Res.* **281**, 453–472 (2016).

3 Reimink, J. R., Chacko, T., Stern, R. A. & Heaman, L. M. Earth's earliest evolved crust generated in an Iceland-like setting. *Nat. Geosci.* **7**, 529–533 (2014).

4 Moyen, J.-F. The composite Archaean grey gneisses: Petrological significance, and evidence for a non-unique tectonic setting for Archaean crustal growth. *Lithos* **123**, 21–36 (2011).

5 O'Neil, J., Carlson, R. W., Francis, D. & Stevenson, R. K. Neodymium-142 Evidence for Hadean Mafic Crust. *Science* **321**, 1828–1831 (2008).

6 Sole, C. et al. Evidence for Hadean mafic intrusions in the Nuvvuagittuq Greenstone Belt, Canada. *Science* **388**, 1431–1435 (2025).

7 Augland, L. E. & David, J. Protocrustal evolution of the Nuvvuagittuq Supracrustal Belt as determined by high precision zircon Lu–Hf and U–Pb isotope data. *Earth Planet. Sci. Lett.* **428**, 162–171 (2015).

8 Shimojo, M. et al. Occurrence and geochronology of the Eoarchean, ~3.9 Ga, Iqaluk Gneiss in the Saglek Block, northern Labrador, Canada: Evidence for the oldest supracrustal rocks in the world. *Precambrian Res.* **278**, 218–243 (2016).

9 Cates, N. L. & Mojzsis, S. J. Pre-3750 Ma supracrustal rocks from the Nuvvuagittuq supracrustal belt, northern Québec. *Earth Planet. Sci. Lett.* **255**, 9–21 (2007).

10 Nutman, A. P. et al. Fifty years of the Eoarchean and the case for evolving uniformitarianism. *Precambrian Res.* **367**, 106442 (2021).

11 Harley, S. L. & Kelly, N. M. in Developments in Precambrian Geology Vol. 15 (eds van Kranendonk, M. J. et al.) 149–186 (Elsevier, 2007).

12 Liu, D. Y., Nutman, A. P., Compston, W., Wu, J. S. & Shen, Q. H. Remnants of ≥3800 Ma crust in the Chinese part of the Sino-Korean craton. *Geology* **20**, 339–342 (1992).

13 Ge, R., Zhu, W., Wilde, S. A. & Wu, H. Remnants of Eoarchean continental crust derived from a subducted proto-arc. *Sci. Adv.* **4**, eaao3159 (2018).

14 Johnson, T. E. et al. An impact melt origin for Earth's oldest known evolved rocks. *Nat. Geosci.* **11**, 795–799 (2018).

15 Laurent, O. et al. Earth's earliest granitoids are crystal-rich magma reservoirs tapped by silicic eruptions. *Nat. Geosci.* **13**, 163–169 (2020).

16 Rollinson, H. Do all Archaean TTG rock compositions represent former melts? *Precambrian Res.* **367**, 106448 (2021).

17 Guitreau, M., Blichert-Toft, J., Martin, H., Mojzsis, S. J. & Albarède, F. Hafnium isotope evidence from Archean granitic rocks for deep-mantle origin of continental crust. *Earth Planet. Sci. Lett.* **337–338**, 211–223 (2012).

18 Dong, C. et al. New discovery of 3.84–3.64 Ga diverse granitoids in eastern Hebei, North China

Craton: Petrogenesis and significance. *GSA Bull.* **136**, 5249–5261 (2024).
19 O'Neil, J., Boyet, M., Carlson, R. W. & Paquette, J.-L. Half a billion years of reworking of Hadean mafic crust to produce the Nuvvuagittuq Eoarchean felsic crust. *Earth Planet. Sci. Lett.* **379**, 13–25 (2013).
20 Wang, D., Qiu, X.-F. & Carlson, R. W. The Eoarchean Muzidian gneiss complex: Long-lived Hadean crustal components in the building of Archean continents. *Earth Planet. Sci. Lett.* **605**, 118037 (2023).
21 Bennett, V. C., Brandon, A. D. & Nutman, A. P. Coupled ^{142}Nd-^{143}Nd Isotopic Evidence for Hadean Mantle Dynamics. *Science* **318**, 1907–1910 (2007).
22 Rizo, H., Boyet, M., Blichert-Toft, J. & Rosing, M. T. Early mantle dynamics inferred from ^{142}Nd variations in Archean rocks from southwest Greenland. *Earth Planet. Sci. Lett.* **377–378**, 324–335 (2013).
23 Li, C.-F. et al. Differentiation of the early silicate Earth as recorded by ^{142}Nd-^{143}Nd in 3.8–3.0 Ga rocks from the Anshan Complex, North China Craton. *Precambrian Res.* **301**, 86–101 (2017).
24 Liou, P. et al. Long-term isolation of Hadean mantle domains revealed from coupled $^{147-146}$Sm-$^{143-142}$Nd systematics in the eastern North China Craton. *Earth Planet. Sci. Lett.* **638**, 118761 (2024).
25 Bouvier, A. & Boyet, M. Primitive Solar System materials and Earth share a common initial ^{142}Nd abundance. *Nature* **537**, 399–402 (2016).
26 Vervoort, J. D. & Kemp, A. I. S. Isotope Evolution of the Depleted Mantle. *Annu. Rev. Earth Planet. Sci.* **53**, 195–221 (2025).
27 Valley, J. W. et al. 4.4 billion years of crustal maturation: oxygen isotope ratios of magmatic zircon. *Contrib. Mineral. Petrol.* **150**, 561–580 (2005).
28 Chen, R.-X., Zheng, Y.-F. & Xie, L. Metamorphic growth and recrystallization of zircon: Distinction by simultaneous in-situ analyses of trace elements, U–Th–Pb and Lu–Hf isotopes in zircons from eclogite-facies rocks in the Sulu orogen. *Lithos* **114**, 132–154 (2010).
29 Griffin, W. L. et al. The Hf isotope composition of cratonic mantle: LAM-MC-ICPMS analysis of zircon megacrysts in kimberlites. *Geochim. Cosmochim. Acta* **64**, 133–147 (2000).
30 Griffin, W. L. et al. Zircon chemistry and magma mixing, SE China: In-situ analysis of Hf isotopes, Tonglu and Pingtan igneous complexes. *Lithos* **61**, 237–269 (2002).
31 Amelin, Y., Lee, D.-C., Halliday, A. N. & Pidgeon, R. T. Nature of the Earth's earliest crust from hafnium isotopes in single detrital zircons. *Nature* **399**, 252–255 (1999).
32 Ge, R.-F., Wilde, S. A., Zhu, W.-B. & Wang, X.-L. Earth's early continental crust formed from wet and oxidizing arc magmas. *Nature* **623**, 334–339 (2023).
33 Koshida, K., Ishikawa, A., Iwamori, H. & Komiya, T. Petrology and geochemistry of mafic rocks in the Acasta Gneiss Complex: Implications for the oldest mafic rocks and their origin. *Precambrian Res.* **283**, 190–207 (2016).
34 Liou, P. & Guo, J. Generation of Archaean TTG Gneisses Through Amphibole-Dominated Fractionation. *J. Geophys. Res. Solid Earth* **124**, 3605–3619 (2019).
35 Tiepolo, M., Oberti, R., Zanetti, A., Vannucci, R. & Foley, S. F. Trace-Element Partitioning Between Amphibole and Silicate Melt. *Rev. Mineral. Geochem.* **67**, 417–452 (2007).
36 Kemp, A. I. S. et al. Hadean crustal evolution revisited: New constraints from Pb–Hf isotope systematics of the Jack Hills zircons. *Earth Planet. Sci. Lett.* **296**, 45–56 (2010).
37 Amelin, Y., Kamo, S. L. & Lee, D.-C. Evolution of early crust in chondritic or non-chondritic Earth inferred from U–Pb and Lu–Hf data for chemically abraded zircon from the Itsaq Gneiss Complex,

West Greenland. *Can. J. Earth Sci.* **48**, 141–160 (2011).
38 Hiess, J., Bennett, V. C., Nutman, A. P. & Williams, I. S. In situ U–Pb, O and Hf isotopic compositions of zircon and olivine from Eoarchaean rocks, West Greenland: New insights to making old crust. *Geochim. Cosmochim. Acta* **73**, 4489–4516 (2009).
39 Wu, F.-Y., Zhang, Y.-B., Yang, J.-H., Xie, L.-W. & Yang, Y.-H. Zircon U–Pb and Hf isotopic constraints on the Early Archean crustal evolution in Anshan of the North China Craton. *Precambrian Res.* **167**, 339–362 (2008).
40 Vezinet, A. et al. Growth of continental crust and lithosphere subduction in the Hadean revealed by geochemistry and geodynamics. *Nat. Commun.* **16**, 3850 (2025).
41 Rosas, J. C. & Korenaga, J. Rapid crustal growth and efficient crustal recycling in the early Earth: Implications for Hadean and Archean geodynamics. *Earth Planet. Sci. Lett.* **494**, 42–49 (2018).
42 Herzberg, C., Condie, K. & Korenaga, J. Thermal history of the Earth and its petrological expression. *Earth Planet. Sci. Lett.* **292**, 79–88 (2010).
43 Johnson, T. E., Brown, M., Gardiner, N. J., Kirkland, C. L. & Smithies, R. H. Earth's first stable continents did not form by subduction. *Nature* **543**, 239–242 (2017).
44 Smithies, R. H. et al. Oxygen isotopes trace the origins of Earth's earliest continental crust. *Nature* **592**, 70–75 (2021).
45 Moore, W. B. & Webb, A. A. G. Heat-pipe Earth. *Nature* **501**, 501–505 (2013).
46 Gerya, T. V., Stern, R. J., Baes, M., Sobolev, S. V. & Whattam, S. A. Plate tectonics on the Earth triggered by plume-induced subduction initiation. *Nature* **527**, 221–225 (2015).
47 Baes, M., Sobolev, S., Gerya, T., Stern, R. & Brune, S. Plate motion and plume-induced subduction initiation. *Gondwana Res.* **98**, 277–288 (2021).
48 O'Neill, C., Marchi, S., Zhang, S. & Bottke, W. Impact-driven subduction on the Hadean Earth. *Nat. Geosci.* **10**, 793–797 (2017).

Figures

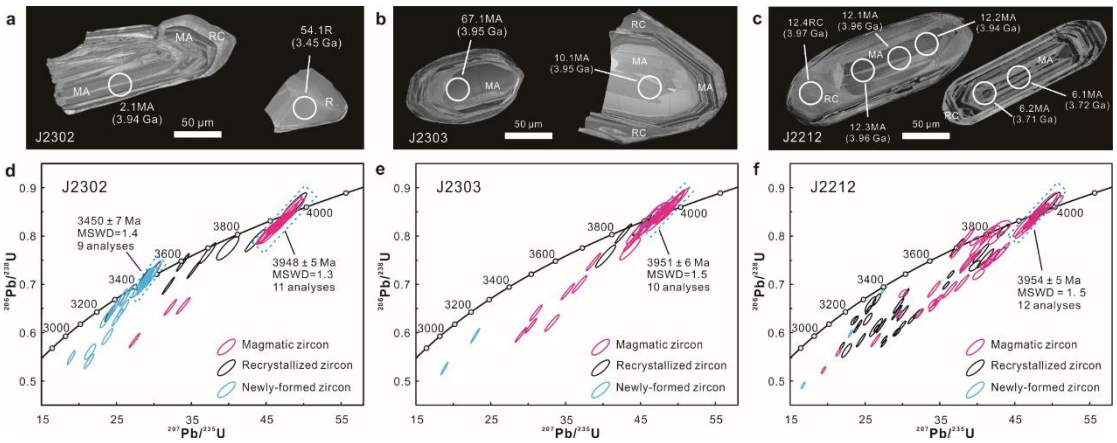


Fig.1. Internal zircon structures and SHRIMP U-Pb data of the 3.95 Ga trondhjemitic gneiss. (a-c) Representative cathodoluminescence (CL) images, showing complex structures and U-Pb ages. MA and RC represent magmatic and recrystallized domains, respectively, whereas R represents overgrowth rims or newly-formed grains during metamorphism. Newly-formed grains are present in sample J2302 (a), whereas magmatic zoning is better preserved in zircon from sample J2303 (b). In the banded trondhjemitic gneiss sample J2212 (c), in addition to the 3.95 Ga magmatic zircons, there are a few younger magmatic zircon grains interpreted to be from intrusive younger granitic veins. Concordia diagrams (d–f) show analyses with discordance less than 20%, all analyses are shown in Fig. S5. The dashed rectangles enclose the grains included in the age calculations.

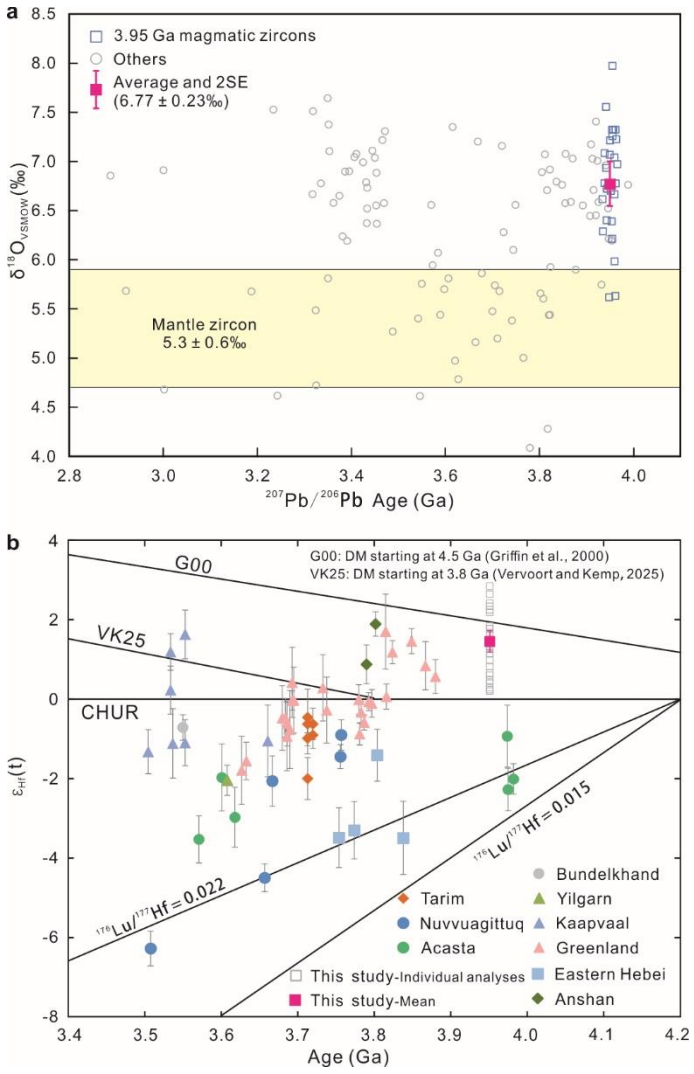


Fig. 2. Zircon Hf-O isotope results for the 3.95 Ga trondhjemitic gneiss. (a) O isotopes of the 3.95 Ga magmatic zircons, with most yielding $\delta^{18}O$ values higher than mantle zircon (5.3 ± 0.6‰, 2SD [27]). The magmatic zircons used for calculating the age of magma crystallization yield an average $\delta^{18}O$ value of 6.77‰ and 2SE of 0.23‰. Other zircons, including 3.95 Ga recrystallized zircons, magmatic/recrystallized zircons with $^{207}Pb/^{206}Pb$ ages younger than 3.95 Ga (due to radiogenic Pb loss), and newly-formed zircons, have similar O isotopic compositions but some show lower values down to 4.09‰. (b) Zircon Hf isotopes of the 3.95 Ga trondhjemitic gneiss, compared with those of other tonalites and trondhjemites older than 3.5 Ga from around the world (Table S8). The gray empty rectangles represent the $\varepsilon_{Hf}(t)$ values of the near concordant analyses with $^{207}Pb/^{206}Pb$ age >3.9 Ga, while the carmine solid rectangle and error bar represent the weighted mean of these analyses (1.45 ± 0.27, 95% confidence level, n = 26, MSWD = 1.5). For other >3.5 Ga TTGs, each symbol represents the average and 2SE of a single sample. Samples where the $\varepsilon_{Hf}(t)$ variation range of magmatic zircon is >8 (or 2SE >1) are not shown, as the large variations may indicate analytical problems or heterogeneous sources. Potassic granites and granodiorites are also not shown due to their more complex formation processes. The DM evolution lines starting from 4.5 Ga [29] (G00) and 3.8 Ga [26] (VK25) are shown, Hf isotopic evolution lines for average crust ($^{176}Lu/^{177}Hf$ = 0.015 [30]) and mafic crust ($^{176}Lu/^{177}Hf$ = 0.022 [31]) are also shown.

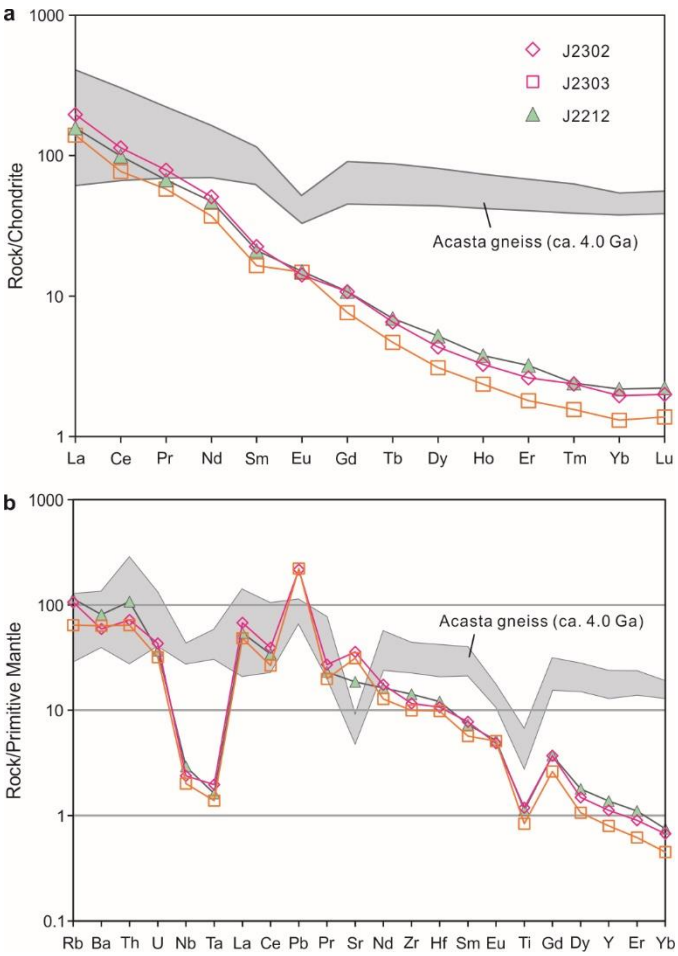


Fig. 3. Rare earth element (REE) pattern (a) and primitive mantle spidergram (b) of the three samples of 3.95 Ga trondhjemitic gneiss, revealing high Sr and low Y, HREE, Nb, Ta, and Ti concentrations, and negligible negative Eu anomalies. This signature is characteristic of high-pressure TTG rocks and contrasts sharply with that of the oldest (ca. 4.0 Ga) Acasta gneiss [2,3] (gray shaded area in both (a) and (b)).

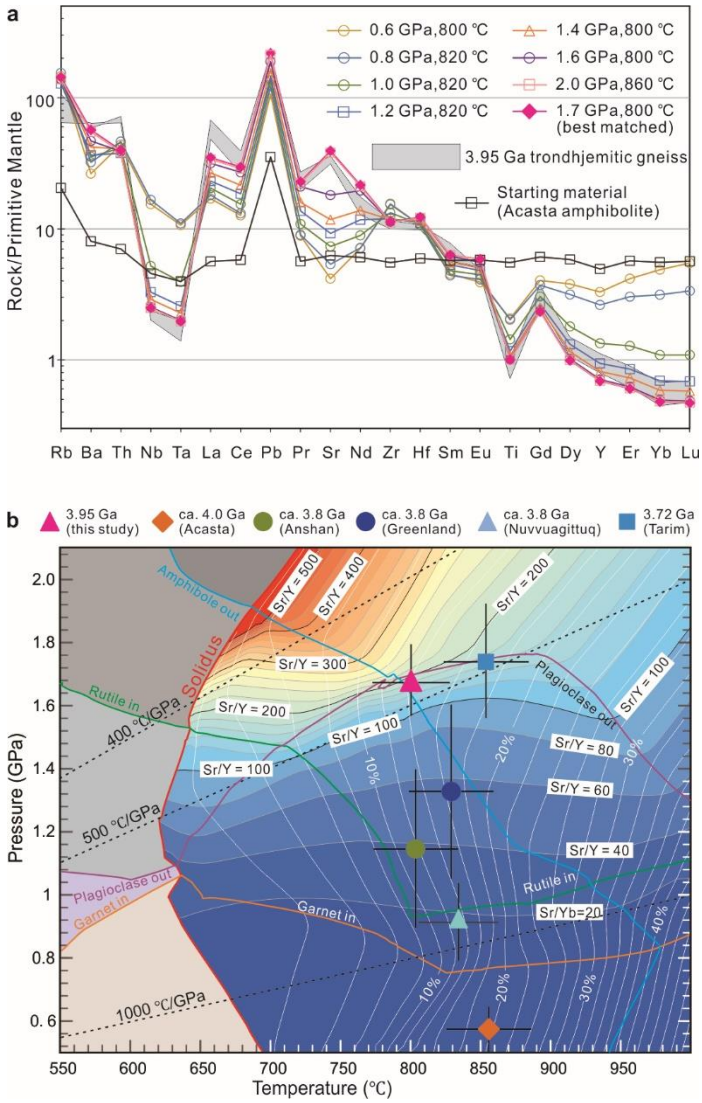


Fig. 4. Thermodynamic partial melting modelling. (a) Comparing the trace element patterns of the 3.95 Ga trondhjemitic gneiss with modelled melts at different P-T conditions using amphibolite group I at Acasta as the starting material, with $X(H_2O)$ = 1.5 wt.% and $Fe^{3+}/(Fe^{3+} + Fe^{2+})$ = 0.1. The P-T conditions for the matched melts are >1.6 GPa and 740 to 860 °C, with the best fit at 1.7 GPa and 800 °C. Melts derived from lower pressure at 0.6-1.0 GPa have weak Nb and Ta negative anomalies and high HREE content, which are significantly different from the 3.95 Ga trondhjemitic gneiss. The melts formed at 1.2-1.4 GPa also have relatively high Nb, Ta, Ti contents. More importantly, the melts formed at these pressures show negative Sr anomalies, which is inconsistent with the positive Sr anomalies in the 3.95 Ga trondhjemitic gneiss. (b) P-T phase diagram for the composition of amphibolite group I from Acasta, assuming $X(H_2O)$ = 1.5wt.% and $Fe^{3+}/(Fe^{3+} + Fe^{2+})$ = 0.1. Simplified from Fig. S9c. Colored isolines of Sr/Y ratio in the melt are displayed on the right side of the solidus, together with the percentage contour lines of the melt (white lines). The Sr/Y ratio of the melt is mainly controlled by pressure, while the degree of partial melting is mainly related to temperature. Inferred P-T conditions and error bars are also shown for some of the oldest rocks in other areas. The pressure is mainly determined by the variation range of Sr/Y ratio, while the temperature is broadly limited by factors closely related to the degree of melting, such as SiO_2 and LILE contents and Na_2O/K_2O ratios. Due to possible variations of parameters in modelling, such as the element compositions of the mafic precursor, water contents and oxygen

fugacity during the formation of the TTGs, the estimation of the P-T conditions may have significant uncertainty. However, it can still reflect the significant differences in pressure and geothermal gradients for the Eoarchean rocks.

MATERIALS AND METHODS

Zircon SHRIMP U-Pb dating

Zircon dating was carried out using the SHRIMP II ion microprobe in the Beijing SHRIMP Center, Chinese Academy of Geological Sciences, Beijing. Unknown zircons were mounted together with two zircon standards TEMORA-2 [49] and 91500 [50] or LDG13 (laboratory standard, Liu, J.H., unpublished data), and then the mount was polished to expose the internal parts of the grains. Cathodoluminescence (CL) images were used to reveal internal structures and assist in selecting appropriate analysis positions. The analytical procedures and conditions were similar to those described by ref. 51. The intensity of the primary O^{2-} beam was ca. 3 nA and analytical spots were nearly circular with a diameter of ~25 μm. Each site was rastered for 3 minutes prior to analysis to remove surface common Pb. Five scans through the mass range were made for data collection. Mass resolution during the analytical sessions was ~5000 (1% peak height). Standard zirconTEMORA-2 [49] was used for calibration $^{206}Pb/^{238}U$ ratios, where M257 (U: 840 ppm [52]) on a separate mount was used to calibrate U contents. Common Pb was corrected using the measured ^{204}Pb abundances with the assumption that the common Pb composition is the same as that of Broken Hill lead ore [53]. Data processing was carried out using the SQUID and ISOPLOT programs [54,55]. The uncertainties of individual analyses shown in Table S1 and on the concordia diagrams are at 1σ. Only the analyses with discordance <5% were used to calculate weighted mean $^{207}Pb/^{206}Pb$ ages and the uncertainties on weighted mean ages are quoted at the 95% confidence level.

Zircon O isotope analysis

Zircon O isotopes were measured at the same locations as the U-Pb analysis using the SHRIMP-IIe SIMS in the Beijing SHRIMP Center. Before O isotope analysis, the mounts were re-polished to remove the previous analysis pits, ensuring removal of any oxygen implanted in zircon from the O^{2-} beam during U-Pb dating. The analytical process was similar to that described in refs. 56 and 57. A primary $^{133}Cs^{+}$ beam was accelerated at ~15 KV and bombarded the zircon surface to produce negative secondary ions. An electron gun prevented the accumulation of positive charge on the zircon surface. The intensity of the Cs+ primary ion beam was 2–3 nA, and the beam intensity of the electron gun was about 0.5 μA. The analysis spots are nearly circular with a diameter of ~25 μm. Prior to analysis of each spot, the zircon was rastered for 2–3 minutes to remove the gold coat and any other contamination and to ensure the secondary beam stabilizes before data collection. The O isotopes were measured in two sets of six scans in static multicollection mode for ^{18}O and ^{16}O, and the count rate for secondary $^{16}O^{-}$ ion was over 10^9 cps. Measured $^{18}O/^{16}O$ ratios were normalized by using Vienna Standard Mean Ocean Water compositions (V-SMOW). Two standard zircons were used to monitor the analyses, with TEMORA-2 ($\delta^{18}O_{V\text{-}SMOW}$ = 8.2‰ [49]) used as a primary standard to monitor the stability of the instrument, and zircon 91500 ($\delta^{18}O_{V\text{-}SMOW}$ = 9.86 ± 0.37‰ [50]) or LDG13 (laboratory standard, $\delta^{18}O_{V\text{-}SMOW}$ = 6.78 ± 0.08‰; Liu, J.H., unpublished data) as a secondary standard to monitor the reliability

of analytical results. TEMORA-2 was analyzed 3 or 4 times at the beginning of each analytical session, then after every 3 or 4 unknowns. Standard 91500 or LDG13 were analyzed after each 4 or 5 TEMORA-2 analyses. Throughout the entire analytical process, the range of $\delta^{18}O_{V\text{-}SMOW}$ values in all 78 TEMORA-2 analyses was between 7.42 and 8.97‰. The weighted mean $\delta^{18}O_{V\text{-}SMOW}$ values for 91500 and LDG13 were 10.01 ± 0.22‰ (2σ, MSWD = 1.3, n = 8) and 6.72 ± 0.25‰ (MSWD = 1.3, n = 7), respectively, consistent with the recommended values within uncertainty.

Zircon trace elements analysis

Zircon trace elements were analyzed at the same locations as the SHRIMP U-Pb and O isotope analysis, using a Cameca IMS-1300HR^3 ion microbe at Nanjing University (Sample J2212) or SHRIMP-IIa in the Beijing SHRIMP Center (Sample J2302 and J2303). The previous analysis pits were removed by re-polishing before analysis. For Cameca analysis, a ~5 nA primary O_2^- beam was utilized to analyze the zircon with 23 keV impact energy. The beam size was about 15 × 20 μm. Measurement was conducted in the mono-collector mode, and each spot analysis includes 5 scan cycles. The following mass sequences were measured: ^{31}P, ^{48}Ti, ^{56}Fe, ^{89}Y, ^{93}Nb, ^{139}La, ^{140}Ce, ^{141}Pr, ^{142}Nd, ^{147}Sm, ^{153}Eu, ^{158}Gd, ^{159}Tb, ^{163}Dy, ^{165}Ho, ^{167}Er, ^{169}Tm, ^{174}Yb, ^{175}Lu, ^{180}Hf, and the intensities were normalized to $^{30}Si^{16}O$. Mass resolution during the analytical sessions was >15,000 (10% peak height). The concentrations of trace elements were standardized against zircon standard 91500 [58], which recorded relative standard deviations of <15% for all elements except for La, Pr and Fe. For SHRIMP analysis, a ~4 nA primary O_2^- beam with a ~25 μm spot diameter was used. Each spot was analyzed using 5 scans. The following mass sequences were measured: ^{64}TiO, ^{89}Y, ^{139}La, ^{140}Ce, ^{141}Pr, ^{146}Nd, ^{147}Sm, ^{151}Eu, ^{157}Gd, ^{159}Tb, ^{163}Dy, ^{165}Ho, ^{167}Er, ^{169}Tm, ^{174}Yb, ^{175}Lu, and the intensities were normalized to $^{90}Zr^{28}Si^{16}O$. The mass resolution was >5,000 at 1% peak height. The concentrations of trace elements were standardized against zircon standard 91500, which had relative standard deviations of <20% for all elements except for La and Pr.

Zircon Lu-Hf isotopic analysis

Zircon Lu-Hf isotopes were measured at the same locations as the U-Pb, O and REE analysis. The mounts were slightly re-polished before analysis. Two sets of analyses were performed. The first analyses were conducted using a Nu Plasma II MC-ICP-MS instrument (Nu Instruments Ltd., UK) connected to a 193 nm ArF laser ablation system (RESOlution M-50, ASI) at Northwest University, Xi'an, China, following the process described in refs. 59 and 60. The second analyses were conducted using a Neptune Plus MC-ICP-MS (Thermo Scientific) connected to a 193 nm ArF laser ablation system (RESOlution S155, ASI) at Wuhan Center of China Geological Survey, following the process described in ref. 20. The spot size was 44 μm and 43μm, respectively. The laser repetition rate was 6 Hz and the energy density applied was 6 J/cm^2 (the first analyses) or 4 J/cm^2 (the second analyses). Each measurement included 30 s background measurement, 45 s (the second analyses) or 60 s (the second analyses) data acquisition, and 40 s washout. The mass fractionation was corrected according to

an exponential law and was normalized to $^{179}Hf/^{177}Hf = 0.7325$ [61]. The isobaric interference of ^{176}Lu and ^{176}Yb on ^{176}Hf were corrected using the stable ratios of $^{176}Yb/^{173}Yb = 0.78696$ [62] and $^{176}Lu/^{175}Lu = 0.02655$ [63]. Two zircon standards GJ-1 and Mudtank (the first analyses) or Plešovice and FC-1 (the second analyses) were analyzed to monitor the process. The obtained $^{176}Hf/^{177}Hf$ ratios were 0.282012 ± 37 (2SD, n = 19) for GJ-1, 0.282506 ± 35 (2SD, n = 20) for Mudtank, 0.282489 ± 4 (2SD, n = 6) for Plešovice and 0.282188 ± 33 (2SD, n = 14) for FC-1 during the course of this study, consistent with the recommended values within 2σ uncertainty (GJ-1: 0.282013 ± 4; Mudtank: 0.282507 ± 6 [59]; Plešovice: 0.282482 ± 13; FC-1: 0.282183 ± 12 [65]). Importantly, FC-1 has relatively highly $^{176}Lu/^{177}Hf$ ratios (0.0006–0.0016) and $^{176}Yb/^{177}Hf$ ratios (0.0238–0.0656), comparable to those of the studied zircons ($^{176}Lu/^{177}Hf = 0.0002–0.0012$, $^{176}Yb/^{177}Hf = 0.0104–0.0485$), except for one analysis (J2302-2.1MA), ensuring the accuracy of isobaric interference correction. The ^{176}Lu decay constant of 1.867×10^{-11} year^{-1} [66], and the present-day chondritic ratios of $^{176}Hf/^{177}Hf = 0.282785$ and $^{176}Lu/^{177}Hf = 0.0336$ were adopted to calculate the $\varepsilon_{Hf}(t)$ values [67]. The 2σ uncertainty of $\varepsilon_{Hf}(t)$ was calculated after ref. 68.

Whole-rock geochemical analysis

Before crushing, homogeneous portions were hand-picked and visible younger veins were removed, except that the veins in J2212 were too thin and closely-spaced to be completely removed. The selected rock fragments are crushed to around 200 mesh. Whole-rock geochemical analyses were carried out in the Wuhan SampleSolution Analytical Technology Co., Ltd., Wuhan, China. Major elements were analyzed by X-ray fluorescence spectrometry (XRF) (Zsx Primus II, RIGAKU, Japan), and the relative standard deviation (RSD) was less than 2%. Trace element analyses were conducted on an Agilent 7700e ICP-MS, with the analytical uncertainties less than 10% for elements with abundance of <10 ppm, and less than 5% for those >10 ppm.

Thermodynamic and trace element modelling

Given the evolution of basaltic crust over time, identifying a suitable source for the 3.95 Ga trondhjemitic gneiss requires evaluation of known Eoarchean meta-basalts (amphibolites). Currently, spatially extensive ≥3.7 Ga amphibolites are documented in only a few areas, including the Acasta complex (Slave Craton [33]), the Isua supracrustal belt (West Greenland [69,70]), the Nuvvuagittuq Greenstone Belt and the adjacent Ukaliq supracrustal belt (Quebec [71–73]), and the Nulliak unit (Saglek-Hebron Complex, northern Labrador [74]).

In the Acasta area, mafic enclaves hosted in 4.0–3.6 Ga felsic gneisses have been classified into 5 geochemical groups, among which amphibolite group I represents the most primitive composition [33]. Meta-basalts from the Isua belt are broadly divided into depleted (boninite) and undifferentiated types [69,70], whereas mafic meta-volcanic rocks in the Nuvvuagittuq Greenstone Belt were classified into high-Ti, enriched low-Ti and depleted low-Ti units [71,72]; mafic rocks in the Ukaliq supracrustal belt have similar geochemical compositions [73]. Amphibolites of the Eoarchean Nulliak unit occur as enclaves in early Archean granitoids and include both incompatible element-enriched

and depleted varieties [74].

To evaluate potential sources for the 3.95 Ga trondhjemitic gneiss, we compiled geochemical compositions for the 9 types of amphibolites from these localities (Table S7). It is generally assumed that TTG melts are produced by moderate degrees (7–30%) of partial melting of amphibolite, because melts cannot accumulate and be extracted if the degree of melting is too low (<7–8%) [75–77], or are too mafic if the degree of melting is too high (>30%). Within this interval, the abundances of strongly incompatible LILEs can be used to constrain the source compositions for the 3.95 Ga trondhjemitic gneiss (Fig. S9a, b). We found that amphibolite group I from the Acasta complex has the most geochemically similar protolith and are the most appropriate source for the studied TTGs. Moreover, this unit represents the only known amphibolite worldwide with an age >3.95 Ga. Hadean ages proposed for the amphibolites from the Nuvvuagittuq Greenstone Belt are debated, and their Nd isotopic composition and LILE concentrations are not suitable for the 3.95 Ga trondhjemitic gneiss. Consequently, Acasta amphibolite group I was selected as the starting composition for partial melting modelling.

Thermodynamic modelling was carried out using the software GeoPS [78] (version 3.3.2). The thermodynamic database HP622 [79] was used, in combination with the following solution models: silicate melt, amphibole, and clinopyroxene models from ref. 80; garnet, orthopyroxene, ilmenite, biotite, chlorite, mica, cordierite, chloritoid and staurolite models from ref. 81; epidote model from ref. 79, plagioclase model from ref. 82, and spinel model from ref. 83. According to the relatively low fO_2 obtained using the zircon Ce-U-Ti oxybarometer (with an average ΔFMQ of -0.65; Table S4 [84]), the $Fe^{3+}/(Fe^{3+} + Fe^{2+})$ ratio was assumed to be 0.1. The initial water content of the source was estimated by mass balance and assuming constant H_2O/Ce ratio during partial melting [85]. Using the Ce contents of the 3.95 Ga trondhjemitic gneiss and the assumed source (equivalent to Acasta amphibolite group I; Table S7), and the magmatic H_2O contents calculated using the zircon oxybarometer-hygrometer [32], the source H_2O contents of 1.35% and 1.85% are proposed for samples J2302 and J2303, respectively (Table S5). Therefore, a values of $X(H_2O)$ = 1.5 wt.% was used in the modelling. The results are presented in Table S9 and Fig. S9c.

Trace element contents in the melts were modelled using the batch melting equation [86]:

$$C_{melt}/C_{source} = 1/[D + F(1–D)]$$

where C_{melt} and C_{source} represent trace element concentration in melt and source, respectively; D is the bulk partition coefficient; and F is the melt fraction (in weight percent). Partition coefficients used in the modeling (Table S10) were mostly taken from ref. 87, except those for garnet and plagioclase, which were from ref. 88, and Nb, Ta and Ti for rutile that was taken from ref. 89. Muscovite is present when the degree of partial melting is low, and its partition coefficients for K, Rb, Cs and REE were adopted from ref. 90, Ba from ref. 91, and other elements from ref. 92.

References

49 Black, L. P. et al. Improved $^{206}Pb/^{238}U$ microprobe geochronology by the monitoring of a trace-

element-related matrix effect; SHRIMP, ID – TIMS, ELA – ICP – MS and oxygen isotope documentation for a series of zircon standards. *Chem. Geol.* **205**, 115–140 (2004).

50 Wiedenbeck, M. et al. Further Characterisation of the 91500 Zircon Crystal. *Geostand. Geoanal. Res.* **28**, 9–39 (2004).

51 Williams, I. S. in Applications of microanalytical techniques to understanding mineralizing processes Vol. 7 (eds McKibben, M.A. et al.) 1–35 (Reviews in Economic Geology, 1998).

52 Nasdala, L. et al. Zircon M257 - a Homogeneous Natural Reference Material for the Ion Microprobe U-Pb Analysis of Zircon. *Geostand. Geoanal. Res.* **32**, 247–265 (2008).

53 Kinny, P. D. 3820 Ma zircons from a tonalitic Armîsoq gneiss in the Godthåb district of Southern West Greenland. *Earth Planet. Sci. Lett.* **79**, 337–347 (1986).

54 Ludwig, K. R. SQUID 1.02, A User's Manual. Berkeley Geochronology Center Special Publication No.2, pp17 (2001).

55 Ludwig, K. R. User's Manual for Isoplot 3.00: A geochronological toolkit for Microsoft Excel Berkeley Geochronology Center Special Publication No. 4, pp71 (2003).

56 Ickert, R. B. et al. Determining high precision, in situ, oxygen isotope ratios with a SHRIMP II: Analyses of MPI-DING silicate-glass reference materials and zircon from contrasting granites. *Chem. Geol.* **257**, 114–128 (2008).

57 Wan, Y. et al. Extreme zircon O isotopic compositions from 3.8 to 2.5 Ga magmatic rocks from the Anshan area, North China Craton. *Chem. Geol.* **352**, 108–124 (2013).

58 Coble, M. A. et al. Trace Element Characterisation of MAD-559 Zircon Reference Material for Ion Microprobe Analysis. *Geostand. Geoanal. Res.* **42**, 481–497 (2018).

59 Yuan, H.-L. et al. Simultaneous determinations of U–Pb age, Hf isotopes and trace element compositions of zircon by excimer laser-ablation quadrupole and multiple-collector ICP-MS. *Chem. Geol.* **247**, 100–118 (2008).

60 Bao, Z. et al. Comparison of synthetic zircon, high-temperature and high-pressure sintered zircon and fast hot-pressing sintered zircon for in situ hafnium isotope analysis by LA-MC-ICP-MS. *J. Anal. At. Spectrom.* **38**, 2313–2323 (2023).

61 Patchett, P. J. & Tatsumoto, M. A routine high-precision method for Lu-Hf isotope geochemistry and chronology. *Contrib. Mineral. Petrol.* **75**, 263–267 (1981).

62 Thirlwall, M. F. & Anczkiewicz, R. Multidynamic isotope ratio analysis using MC–ICP–MS and the causes of secular drift in Hf, Nd and Pb isotope ratios. *Int. J. Mass Spectrom.* **235**, 59–81 (2004).

63 Vervoort, J. D., Patchett, P. J., Söderlund, U. & Baker, M. Isotopic composition of Yb and the determination of Lu concentrations and Lu/Hf ratios by isotope dilution using MC-ICPMS. *Geochem. Geophy. Geosy.* **5**, Q11002, (2004).

64 Sl̨áma, J. et al. Plešovice zircon — A new natural reference material for U–Pb and Hf isotopic microanalysis. *Chem. Geol.* **249**, 1–35 (2008).

65 Fisher, C. M., Vervoort, J. D. & DuFrane, S. A. Accurate Hf isotope determinations of complex zircons using the "laser ablation split stream" method. *Geochem. Geophy. Geosy.* **15**, 121–139 (2014).

66 Söderlund, U., Patchett, P. J., Vervoort, J. D. & Isachsen, C. E. The 176Lu decay constant determined by Lu–Hf and U–Pb isotope systematics of Precambrian mafic intrusions. *Earth Planet. Sci. Lett.* **219**, 311–324 (2004).

67 Bouvier, A., Vervoort, J. D. & Patchett, P. J. The Lu–Hf and Sm–Nd isotopic composition of CHUR: Constraints from unequilibrated chondrites and implications for the bulk composition of terrestrial

planets. *Earth Planet. Sci. Lett.* **273**, 48–57 (2008).
69 Furnes, H., Rosing, M., Dilek, Y. & de Wit, M. Isua supracrustal belt (Greenland)—A vestige of a 3.8 Ga suprasubduction zone ophiolite, and the implications for Archean geology. *Lithos* **113**, 115–132 (2009).
70 Hoffmann, J. E. et al. Mechanisms of Archean crust formation inferred from high-precision HFSE systematics in TTGs. *Geochim. Cosmochim. Acta* **75**, 4157–4178 (2011).
71 O'Neil, J., Francis, D. & Carlson, R. W. Implications of the Nuvvuagittuq Greenstone Belt for the Formation of Earth's Early Crust. *J. Petrol.* **52**, 985–1009 (2011).
72 O'Neil, J., Carlson, R. W., Papineau, D., Levine, E. Y. & Francis, D. in Earth's Oldest Rocks (Second Edition) (eds van Kranendonk, M. J. et al.) 349–374 (Elsevier, 2019).
73 Caro, G., Morino, P., Mojzsis, S. J., Cates, N. L. & Bleeker, W. Sluggish Hadean geodynamics: Evidence from coupled ^{146,147}Sm–^{142,143}Nd systematics in Eoarchean supracrustal rocks of the Inukjuak domain (Québec). *Earth Planet. Sci. Lett.* **457**, 23–37 (2017).
74 Wasilewski, B., O'Neil, J. & Rizo, H. Geochemistry and petrogenesis of the early Archean mafic crust from the Saglek-Hebron Complex (Northern Labrador). *Precambrian Res.* **328**, 321–343 (2019).
75 Vigneresse, J. L., Barbey, P. & Cuney, M. Rheological Transitions During Partial Melting and Crystallization with Application to Felsic Magma Segregation and Transfer. *J. Petrol.* **37**, 1579–1600 (1996).
76 Brown, M. Crustal melting and melt extraction, ascent and emplacement in orogens: mechanisms and consequences. *J. Geol. Soc. London* **164**, 709–730 (2007).
77 Rosenberg, C. L. & Handy, M. R. Experimental deformation of partially melted granite revisited: implications for the continental crust. *J. Metamorph. Geol.* **23**, 19–28 (2005).
78 Xiang, H. & Connolly, J. A. D. GeoPS: An interactive visual computing tool for thermodynamic modelling of phase equilibria. *J. Metamorph. Geol.* **40**, 243–255 (2022).
79 Holland, T. J. B. & Powell, R. An improved and extended internally consistent thermodynamic dataset for phases of petrological interest, involving a new equation of state for solids. *J. Metamorph. Geol.* **29**, 333–383 (2011).
80 Green, E. C. R. et al. Activity–composition relations for the calculation of partial melting equilibria in metabasic rocks. *J. Metamorph. Geol.* **34**, 845–869 (2016).
81 White, R. W., Powell, R. & Johnson, T. E. The effect of Mn on mineral stability in metapelites revisited: new a–x relations for manganese-bearing minerals. *J. Metamorph. Geol.* **32**, 809–828 (2014).
82 Holland, T. & Powell, R. Activity–composition relations for phases in petrological calculations: an asymmetric multicomponent formulation. *Contrib. Mineral. Petrol.* **145**, 492–501 (2003).
83 White, R. W., Powell, R. & Clarke, G. L. The interpretation of reaction textures in Fe-rich metapelitic granulites of the Musgrave Block, central Australia: constraints from mineral equilibria calculations in the system K_2O–FeO–MgO–Al_2O_3–SiO_2–H_2O–TiO_2–Fe_2O_3. *J. Metamorph. Geol.* **20**, 41–55 (2002).
84 Loucks, R. R., Fiorentini, M. L. & Henríquez, G. J. New Magmatic Oxybarometer Using Trace Elements in Zircon. *J. Petrol.* **61**, egaa34 (2020).
85 Sobolev, A. V. et al. Deep hydrous mantle reservoir provides evidence for crustal recycling before 3.3 billion years ago. *Nature* **571**, 555–559 (2019).
86 Shaw, D. M. Trace element fractionation during anatexis. *Geochim. Cosmochim. Acta* **34**, 237–243

(1970).
87 Bédard, J. H. A catalytic delamination-driven model for coupled genesis of Archaean crust and sub-continental lithospheric mantle. *Geochim. Cosmochim. Acta* **70**, 1188–1214 (2006).
88 Qian, Q. & Hermann, J. Partial melting of lower crust at 10–15 kbar: constraints on adakite and TTG formation. *Contrib. Mineral. Petrol.* **165**, 1195–1224 (2013).
89 Xiong, X. et al. Partitioning of Nb and Ta between rutile and felsic melt and the fractionation of Nb/Ta during partial melting of hydrous metabasalt. *Geochim. Cosmochim. Acta* **75**, 1673–1692 (2011).
90 Hulsbosch, N., Hertogen, J., Dewaele, S., André, L. & Muchez, P. Alkali metal and rare earth element evolution of rock-forming minerals from the Gatumba area pegmatites (Rwanda): Quantitative assessment of crystal-melt fractionation in the regional zonation of pegmatite groups. *Geochim. Cosmochim. Acta* **132**, 349–374 (2014).
91 Icenhower, J. & London, D. An experimental study of element partitioning among biotite, muscovite, and coexisting peraluminous silicic melt at 200 MPa (H_2O). *Am. Mineral.* **80**, 1229–1251 (1995).
92 Raimbault, L. & Burnol, L. The Richemont rhyolite dyke, Massif Central, France; a subvolcanic equivalent of rare-metal granites. *Can. Mineral.* **36**, 265–282 (1998).

Acknowledgements We express our gratitude to Chun Yang for making the zircon mounts; Zemin Bao and Jianhui Liu are thanked for their help with zircon SHRIMP U-Pb-O isotope and trace elements analyses. We also thank Zhi'an Bao, Xiaofei Qiu and Xirun Qiu for assistance in zircon Hf analyses, Xiaolei Wang and Lanlan Tian for zircon Cameca trace elements analyses.

Funding This work was supported by the Key Program of National Natural Science Foundation of China (42130311), National Natural Science Foundation of China (41872200) and the Joint Fund of the National Natural Science Foundation of China (U2344210).

Author contributions Y.W., H.X, C.D., P.L., S.L. and D.L. carried out field work and sample analyses. R.G. and H.X. carried out thermodynamic-trace element modeling. H.X. and C.D. wrote the draft of the manuscript. Y.W., R.G. and S.A.W. improved the text and data interpretation. All the authors contributed towards interpreting and editing of the manuscript.

Competing Interests The authors declare that they have no known competing financial interests or personal relationships that could have appeared to influence the work reported in this paper.

Correspondence and requests for materials should be addressed to Yusheng Wan and Hangqiang Xie.

Supplementary

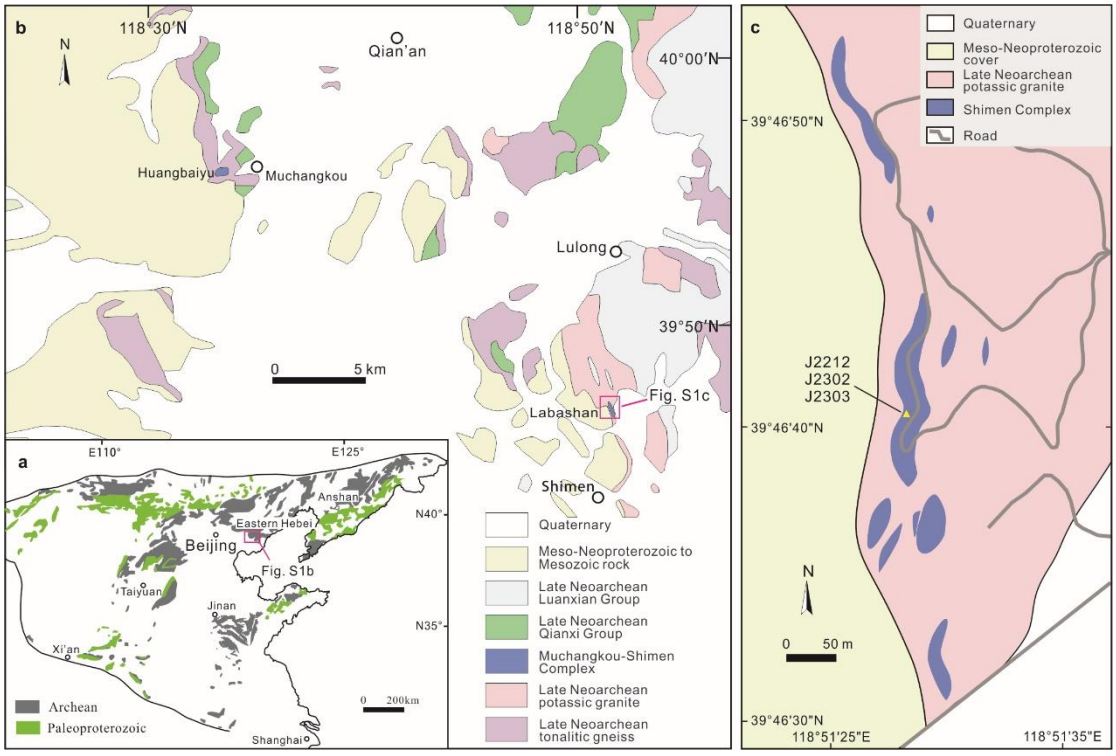


Fig. S1. (a) Geological map of the early Precambrian rocks in the North China Craton [93], showing distribution of Archean and Paleoproterozoic rocks. (b) Geological map of the Qian'an-Lulong area (modified after refs. 94-96), showing the spatial distribution of the early Archean Muchangkou-Shimen Complex. (c) Geological map of the Shimen Complex [18]. The complex is composed of Eo- to Mesoarchean granitoids and supracrustal rocks as enclaves of varying sizes in undeformed 2.5 Ga potassic granite.



Fig. S2. Field photos of the 3.95 Ga trondhjemitic gneiss and related rocks, with sample sites marked. (a) The 3.95 Ga trondhjemitic gneiss is aligned parallel to the foliation in the 3.5 Ga potassic granite gneiss, and is intruded by 2.5 Ga undeformed potassic granite. The locations of samples J2212, J2302 and J2303 are shown. (b) 3.95 Ga banded trondhjemitic gneiss (J2212). The light-colored layers, commonly less than 1 cm in width, are considered to be deformed veins. (c) trondhjemitic gneiss (J2302), (d) trondhjemitic gneiss (J2303). Compared with sample J2212, there are fewer veins in both of the latter, and were removed during sample preparation.

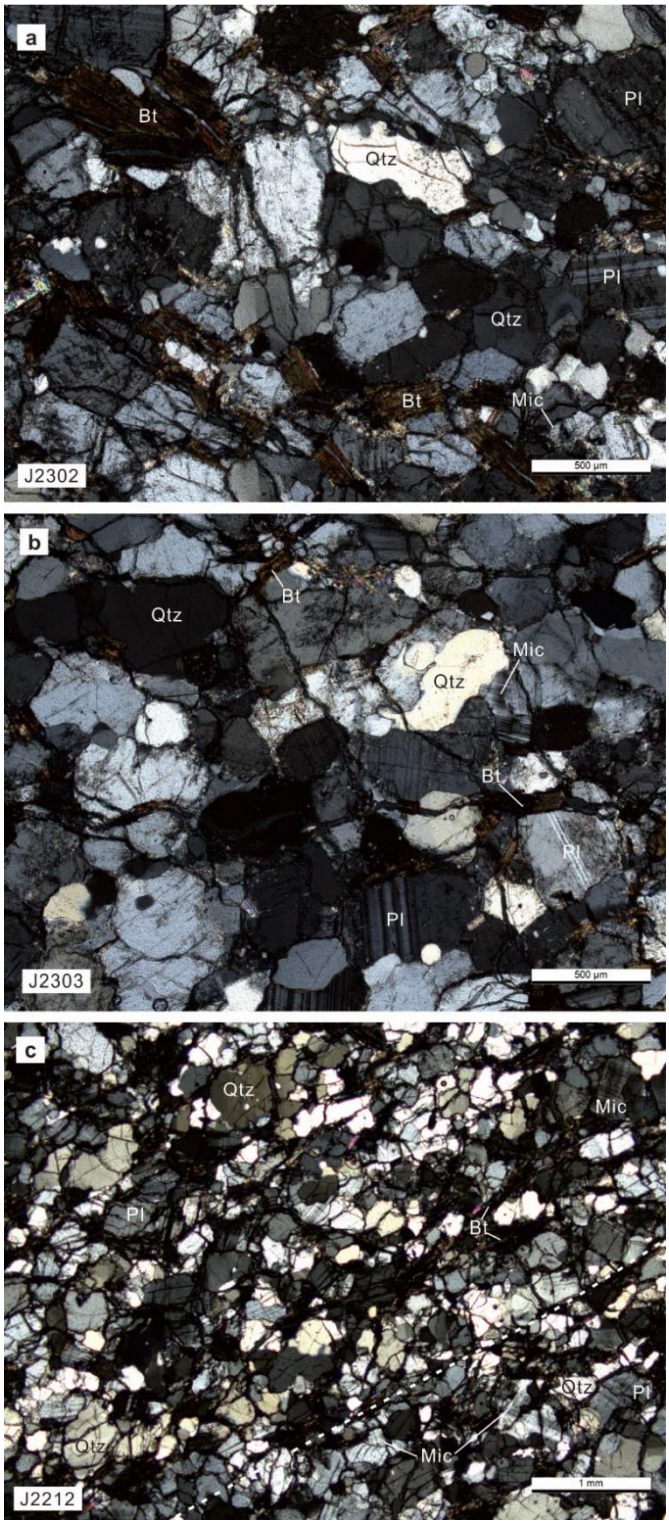


Fig. S3. Photomicrographs of the 3.95 Ga trondhjemitic gneiss. (a) trondhjemitic gneiss (J2302) shows a granoblastic texture and is composed of plagioclase, quartz and biotite, with minor microcline. (b) trondhjemitic gneiss (J2303) has a similar texture and mineral composition to J2302, except for containing less biotite. (c) 3.95 Ga banded trondhjemitic gneiss (J2212) consists of different components. The lower right contains more K-feldspar (monzogranitic layer) compared with the upper left (trondhjemitic layer), consistent with the banded characteristics in the field (Fig. S2b). Both layers show the same foliation defined by oriented biotite flakes.

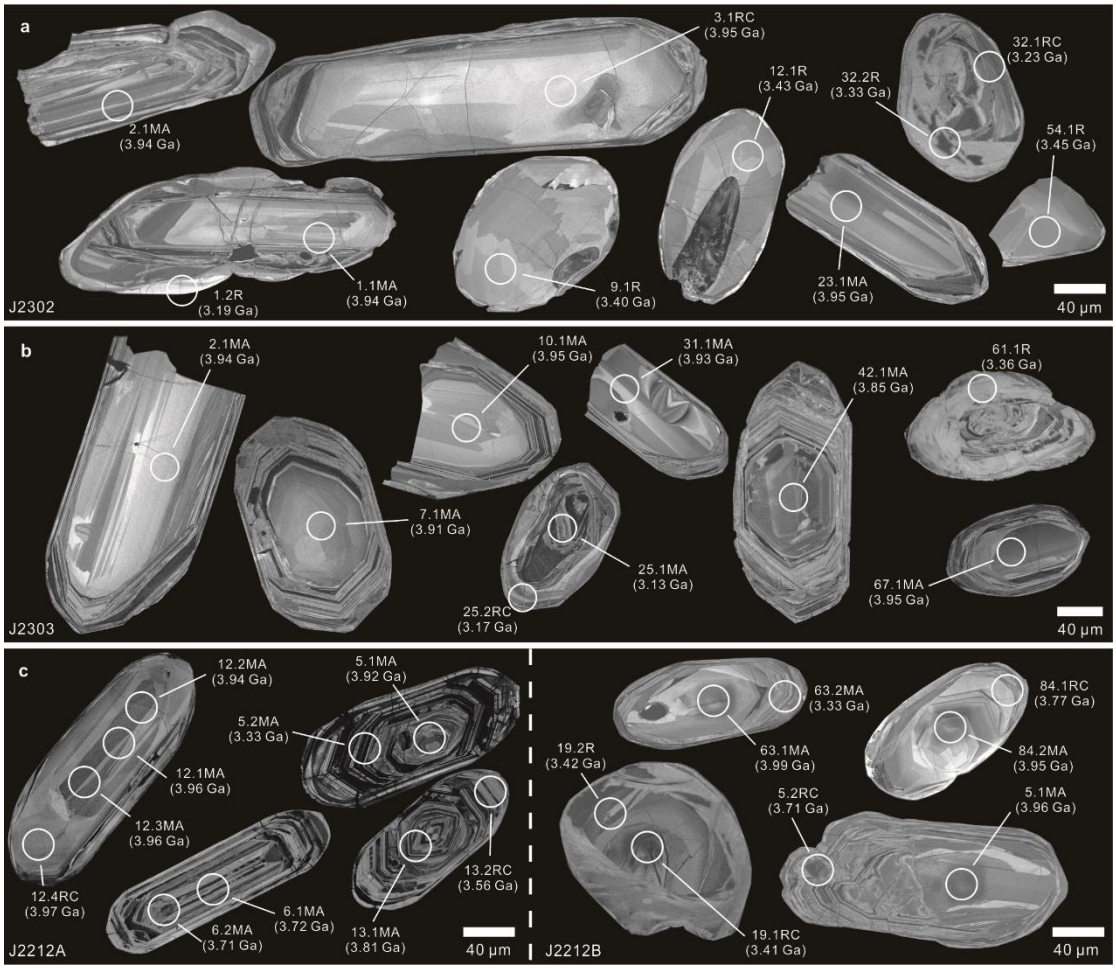


Fig. S4. Cathodoluminescence (CL) images of representative zircons. (a) 3.95 Ga trondhjemitic gneiss (J2302). (b) trondhjemitic gneiss (J2303). (c) Banded trondhjemitic gneiss (J2212, including zircons analyzed in two sessions from the same sample, marked as J2212A and J2212B). MA and RC identify magmatic and recrystallized domains, respectively, whereas R represents overgrowth rims and newly-formed grains during metamorphism. The analytical sites are marked with white circles, together with the analysis number and age.

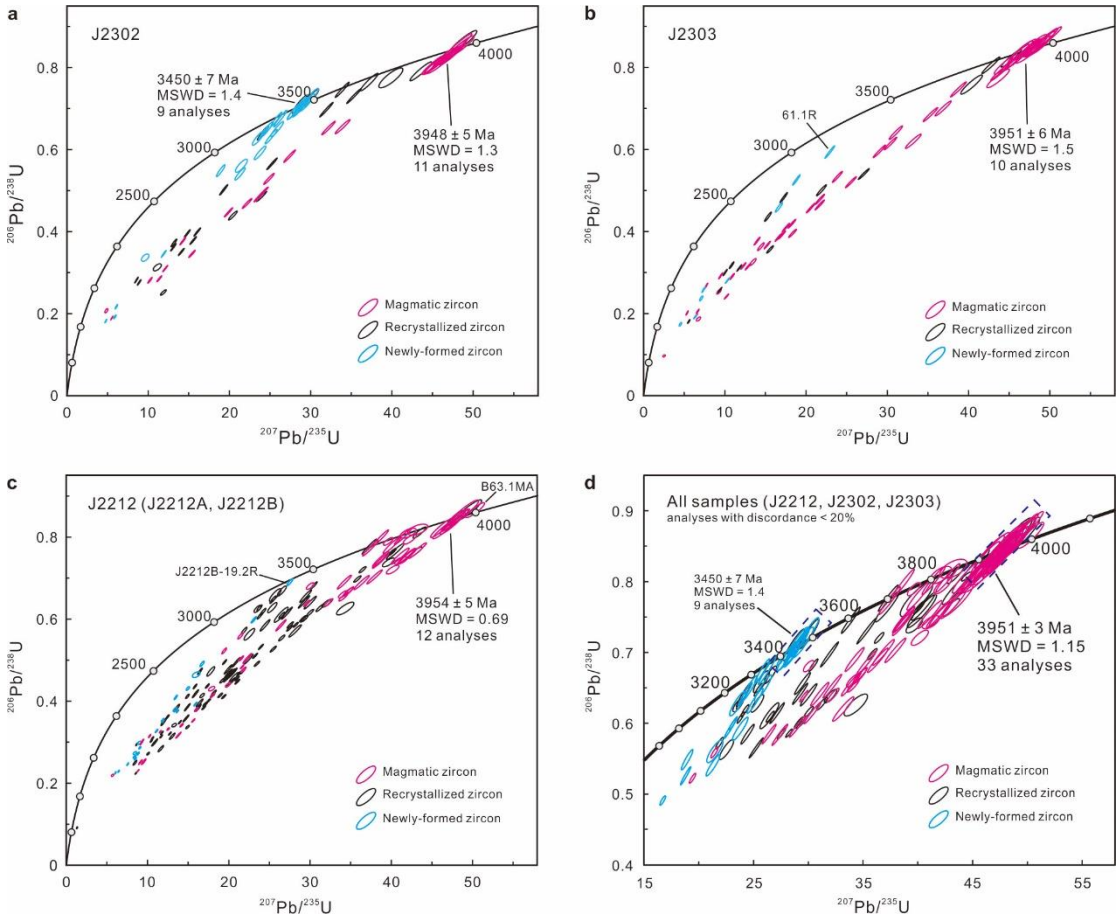


Fig. S5. Concordia diagrams showing the full set of SHRIMP U-Pb zircon analyses. (a) Zircon analyses of trondhjemitic gneiss sample J2302 define two concordant age groups at 3.95 Ga and 3.45 Ga, interpreted as the timing of magmatic crystallization and subsequent metamorphism, respectively. (b) Most zircons in trondhjemitic gneiss sample J2303 are magmatic and cluster near 3.95 Ga. Overgrowth rims show Pb* loss, including analysis 61.1R, which is the closest to concordia. (c) Zircon analyses from banded trondhjemitic gneiss sample J2212 (including zircons analyzed in two sessions from the same sample, marked as J2212A and J2212B) are more scattered, with the main population along a discordia line from 3.95 Ga. However, a few zircons with magmatic zoning yield concordant ages of 3.86–3.70 Ga, potentially due to the intrusion of thin granitic veins or ancient Pb* loss from 3.95 Ga zircons. Analysis 63.1MA in J2212B has the oldest $^{207}Pb/^{206}Pb$ age of 3989 ± 10 Ma, but shows slightly reverse discordance, likely due to local enrichment of radiogenic Pb during later metamorphism [97]. (d) Concordia diagram of all samples for analyses with <20% discordance. The weighted mean $^{207}Pb/^{206}Pb$ age of 3951 ± 3 Ma (2σ, MSWD = 1.15, n = 33) for magmatic/recrystallized cores is considered the best estimate for the magmatic crystallization age of the trondhjemitic gneiss.

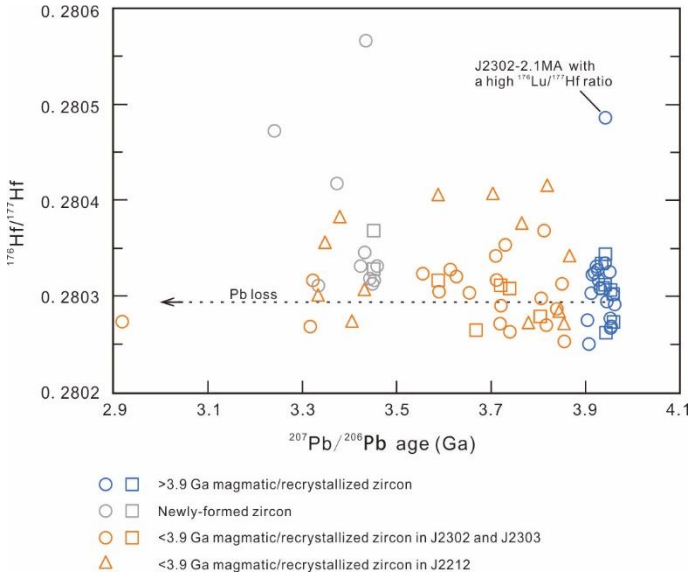


Fig. S6. Zircon Hf isotopes of the 3.95 trondhjemitic gneiss plotted against $^{207}Pb/^{206}Pb$ age. Circles and triangles represent the results of the first analysis, whereas squares represent the results of the second analytical session. All of the magmatic/recrystallized zircons with >3.9 Ga $^{207}Pb/^{206}Pb$ age have homogeneous $^{176}Hf/^{177}Hf$ ratios except for J2302-2.1MA, which has a high $^{176}Lu/^{177}Hf$ ratio. The magmatic/recrystallized zircons with <3.9 Ga $^{207}Pb/^{206}Pb$ age in samples J2302 and J2303 are all located near the Pb loss line. Some newly-formed zircons have significantly higher $^{176}Hf/^{177}Hf$ ratios, which may be related to external fluids during metamorphism.

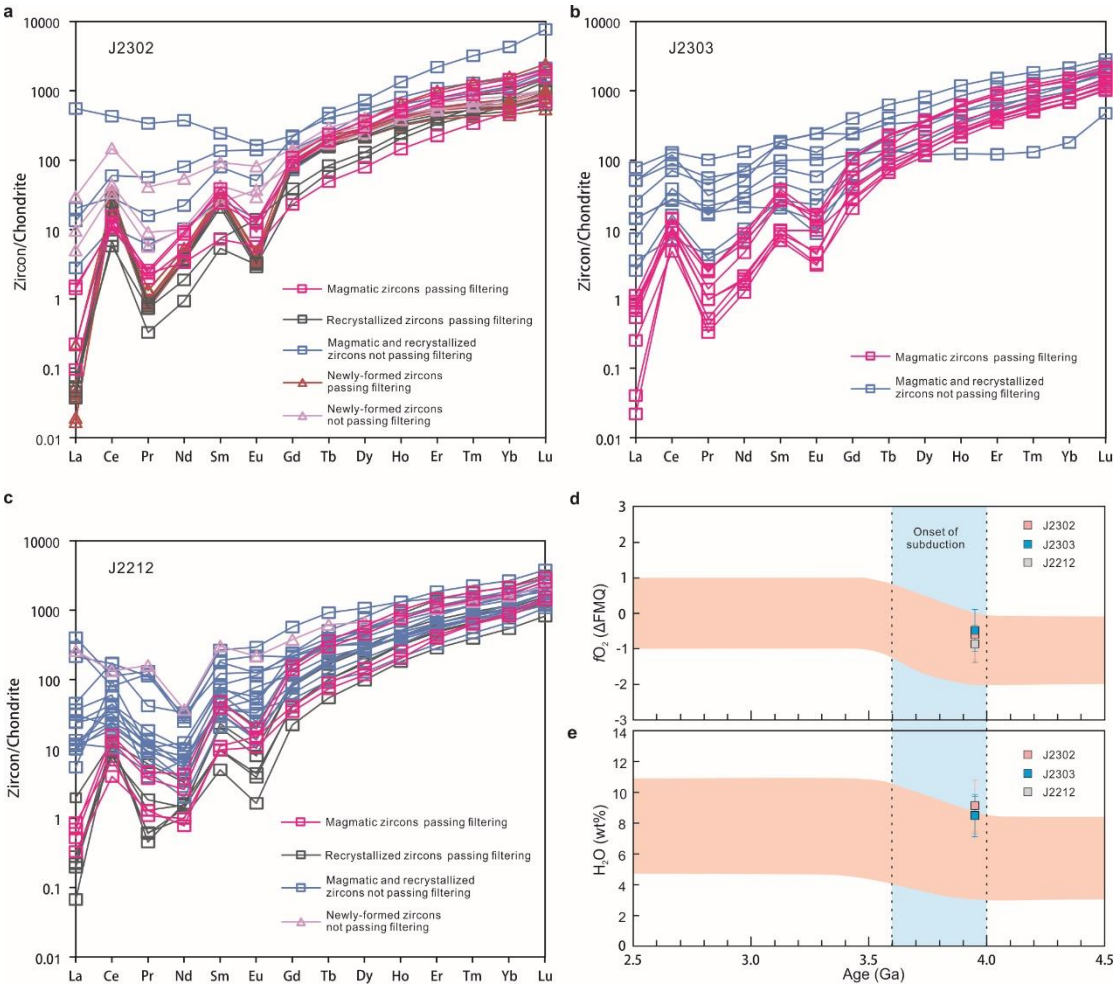


Fig. S7. (a), (b) and (c) REE patterns of zircons from the 3.95 Ga trondhjemitic gneiss (sample J2302, J2303, and J2212). The REE data were filtered using the methods suggested by ref. 32. (d) and (e) Magmatic oxygen fugacity and H_2O content of the 3.95 trondhjemitic gneiss. The oxygen fugacity (fO_2) was calculated using the oxybarometer proposed by ref. 83 based on the average REE content of the filtered magmatic zircons. The magmatic water content was calculated using the hygrometer established by ref. 32, and the effect of U loss in the whole-rock was corrected assuming a Th/U ratio of 5 [32]. Considering that the composition of sample J2212 may have been influenced by the alteration and intrusion of thin younger veins, the average composition of J2302 and J2303 was used for calculating the fO_2 and water content of J2212.

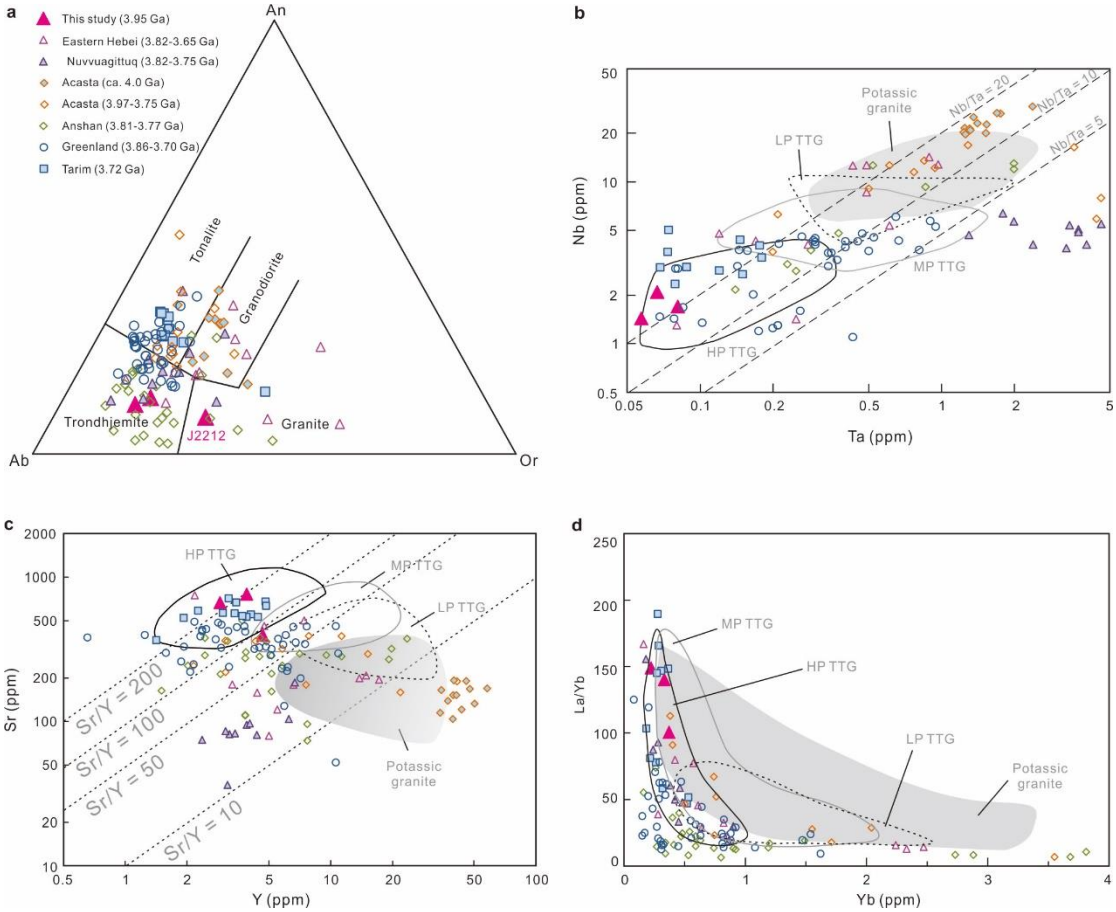


Fig. S8. Geochemical comparison between the 3.95 Ga trondhjemitic gneiss and >3.7 Ga TTG around the world. (a) An-Ab-Or diagram [98]. The 3.95 Ga trondhjemitic gneiss (sample J2212 plots in the granite field due to thin younger granitic veins) is similar to the granitoids in Anshan and Nuvvuagittuq (mainly trondhjemitic gneiss), but different from those in Acasta, Tarim and Greenland (mainly tonalitic and granodioritic gneisses). (b) Nb vs. Ta diagram, (c) Sr vs. Y diagram, (d) La/Yb vs. Yb classification diagrams for high-pressure (HP), medium-pressure (MP) and low-pressure (LP) TTGs [4]. The 3.95 trondhjemitic gneiss consistently plots in the HP TTG field, being similar to the 3.72 Ga Aktash gneiss in Tarim and some TTG rocks in Greenland, but different from many other ≥3.8 Ga granitoids around the world, which mostly plot into the MP and LP TTG fields. A few samples outside the ranges in figures b and d are not displayed.

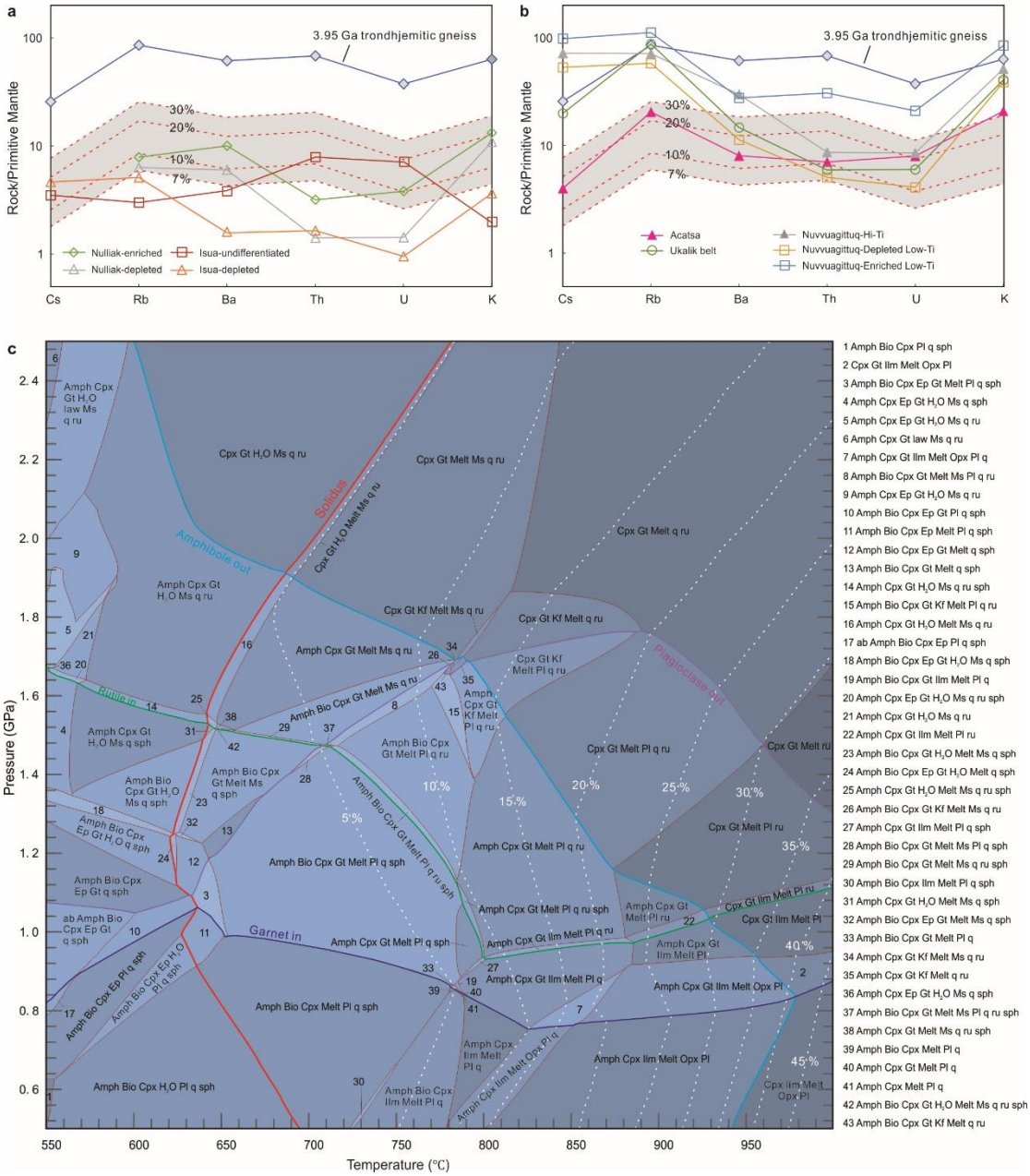


Fig. S9. Thermodynamic and trace element modelling. (a) and (b) LILE contents of the 3.95 Ga trondhjemitic gneiss and potential source rocks (Table S6 and S7). The red dashed lines represent LILE contents required for the source to produce the 3.95 Ga trondhjemitic gneiss by 7, 10, 20 and 30% melting, assuming these elements are perfectly incompatible with bulk partition coefficient = 0. Considering that the degree of partial melting of a mafic rock source needs to be >7% for melt aggregation to form magma, but <30% to match the high SiO_2 contents of the 3.95 Ga trondhjemitic gneiss, the LILE contents of the source need to be in the gray shaded area. Since the sources of Eoarchean TTGs are from mafic rocks, we have compiled the geochemical data of Eoarchean mafic rocks worldwide (see Methods, and Table S7). Comparing the LILE contents of these mafic rocks with those required to form the 3.95 trondhjemitic gneiss, the amphibolite group I in Acasta is the most suitable source, consistent with the fact that it is the only mafic rock >3.95 Ga. (c) P-T pseudosection for the composition of amphibolite group I in Acasta. Assuming $X(H_2O)$ = 1.5 wt.% and $Fe^{3+}/(Fe^{3+} + Fe^{2+})$ ratio = 0.1. The white dashed lines represent the wt.% of melt.

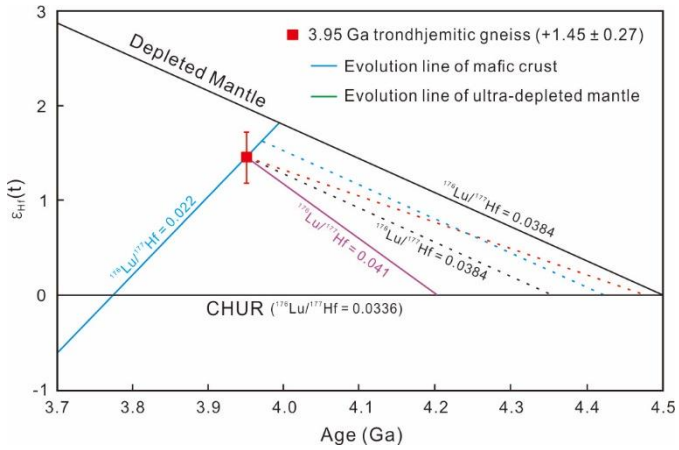


Fig. S10. Hf isotope evolution diagram. The positive $\varepsilon_{Hf}(t)$ values of magmatic zircons from the 3.95 Ga trondhjemitic gneiss indicate that its basaltic precursor was young juvenile crust derived from the DM. Even if the basaltic precursor (assuming $^{176}Lu/^{177}Hf = 0.022$) was derived from a 4.5 Ga DM with the similar $^{176}Lu/^{177}Hf$ ratio (0.0384) to modern DM, its extraction time from the mantle could not be earlier than 4.0 Ga (blue solid line). If the 3.95 Ga trondhjemitic gneiss was formed by partial melting of basalt immediately extracted from DM with similar $^{176}Lu/^{177}Hf$ ratio, then the timing of mantle depletion can be estimated to be ca. 4.35 Ga (black dashed line). Earlier depletion of the mantle is required if partial melting of a basaltic precursor occurred some time after its extraction from DM (blue dashed line) or the degree of depletion in the mantle is less than modern DM (red dashed line). If the basaltic precursor was derived from a possible ultra-depleted mantle proposed by some researchers [99], the depletion can be slightly delayed. Nevertheless, the depletion still needs to be no later than 4.2 Ga even if the $^{176}Lu/^{177}Hf$ of the ultra-depleted mantle is as high as 0.041 (purple solid line). Therefore, Hadean DM is necessary to yield the Hf isotope composition of the 3.95 Ga trondhjemitic gneiss.

Reference

93 Wan, Y.S. et al. Early Neoarchean (~2.7 Ga) tectono-thermal events in the North China Craton: A synthesis. *Precambrian Res.* **247**, 45–63 (2014).

94 Chu, H. et al. The geological significance of the rediscovered fuchsite quartzite with abundant Eoarchean detrital zircons in eastern Hebei Province. *Chin. Sci. Bull*. **61**, 2299–2308 (In Chinese with English abstract). (2016).

95 Wan, Y.S. et al. Discovery of early Eochean-Hadean zircons in eastern Hebei, North China Craton. *Acta Geol. Sin.* **95**, 277–291 (In Chinese with English abstract). (2021).

96 Wan, Y.S. et al. Discovery of ~3.8 Ga TTG rocks in eastern Hebei, North China Craton. *Acta Geol. Sin.* **95**, 1321–1333 (In Chinese with English abstract). (2021).

97 Ge, R.F. et al. A 4463 Ma apparent zircon age from the Jack Hills (Western Australia) resulting from ancient Pb mobilization. *Geology* **46**, 303–306, doi:10.1130/g39894.1 (2018).

98 Barker, F. in Trondhjemites, Dacites and Related Rocks (ed Barker, F.) 1–12 (Elsevier, 1979).

99 Stracke, A., Genske, F., Berndt, J. & Koornneef, J. M. Ubiquitous ultra-depleted domains in Earth's mantle. *Nat. Geosci.* **12**, 851–855 (2019).

Supplementary Files

This is a list of supplementary files associated with this preprint. Click to download.

- XieetalSupplementaryTableFinal.xlsx